SIMULATION MODELING OF AN EARTH ENTRY SYSTEM AND SOLAR RADIATION PRESSURE MODULE DEVELOPMENT

by

Michael Sean Manwell
Bachelors of Science, Mechanical Engineering, Old Dominion University

A Project Report Submitted to the Faculty of Old Dominion University in
Partial Fulfillment of the Requirement for the Degree of

MASTER OF ENGINEERING
in
AEROSPACE ENGINEERING

DEPARTMENT OF MECHANICAL AND AEROSPACE ENGINEERING

OLD DOMINION UNIVERSITY
August 2024



ME-22-0192

SIMULATION MODELING OF AN EARTH ENTRY SYSTEM AND SOLAR RADIATION PRESSURE MODULE DEVELOPMENT

by

Michael Sean Manwell
Bachelors of Science, Mechanical Engineering, Old Dominion University

A Project Report Submitted to the Faculty of Old Dominion University in
Partial Fulfillment of the Requirement for the Degree of

MASTER OF ENGINEERING
in
AEOSPACE ENGINEERING

DEPARTMENT OF MECHANICAL AND
AEROSPACE ENGINEERING

OLD DOMINION UNIVERSITY
August 2024

Approved By:

_____
Dr. Brett Newman (Advisor)

_____
Dr. Gene Hou (Member)

_____
Dr. Colin Britcher (Member)

ABSTRACT

SIMULATION MODELING OF AN EARTH ENTRY SYSTEM AND SOLAR RADIATION PRESSURE MODULE DEVELOPMENT

Michael Sean Manwell
Old Dominion University, 2024
Advisor: Dr. Brett Newman

Several trajectory simulation tools are used to model different phases of the Approach, Entry, Descent and Landing (AEDL) phase of NASA's Mars Sample Return Campaign. Working towards a single simulation tool that models all AEDL phases, this project utilizes Program to Optimize Simulated Trajectories II to simulate the 72-hour exoatmospheric phase of AEDL up till the point of Earth atmospheric entry. This involves developing a new feature for POST2 that captures the forces and moments caused by solar radiation pressure (SRP). Generalizing the vehicle geometry as a combination of primitive shapes, a generalized SRP module was created and implemented into POST2. Trajectory solutions produced by POST2 were then successfully compared against independent solutions produced by the trajectory tool 42.

NOMENCLATURE

State Elements

X_{bc} Position along x-axis in Body frame
Y_{bc} Position along y-axis in Body frame
Z_{bc} Position along z-axis in Body frame
X_{FM} Position along x-axis in Flight Mechanic frame (FM)
Y_{FM} Position along y-axis in Flight Mechanic frame
Z_{FM} Position along z-axis in Flight Mechanic frame
X_{J2000}, X_{eme} Position along x-axis in Earth's Mean Equator and Equinox 2000 frame (J2000)
Y_{J2000}, Y_{eme} Position along y-axis in Earth's Mean Equator and Equinox 2000 frame
Z_{J2000}, Z_{eme} Position along z-axis in Earth's Mean Equator and Equinox 2000 frame
X_I, XI Position along x-axis in Earth Centered Inertial frame (ECI)
Y_I, YI Position along y-axis in Earth Centered Inertial frame
Z_I, ZI Position along z-axis in Earth Centered Inertial frame
$\vec{r}_{Sun \to Sat.}$ Position vector of satellite with respect to Sun
$\hat{r}_{Sun \to Sat.}$ Position unit vector of satellite with respect to Sun
$r_{Sun \to Sat.}$ Radius of satellite with respect to Sun
ϕ Roll angle
θ Pitch angle
ψ Yaw angle
$\vec{a}_g$ Gravitational acceleration of Earth's gravity modeled as an oblate spheroid
$\vec{a}_{3B}$ Acceleration due to 3rd body perturbations of celestial bodies
$\vec{a}_{fm}$ Acceleration in FM frame
$\vec{\omega}_{fm}$ Angular velocity in FM frame
$\vec{\alpha}_{fm}$ Angular acceleration in FM frame
ω_E Earth's angular velocity constant

Solar Radiation Pressure Elements

$\hat{S}$ Solar unit vector of the satellite with respect to the Sun
β Solar sideslip angle
P_s Solar radiation pressure
ϕ_s Solar heat flux
k_{1AU} Solar heat flux at one astronomical unit
AU Astronomical Unit
α Solar angle of attack
c Speed of light constant
$\vec{F}_{S_{Logic}}$ Logic gate used by 42 to calculate forces due to solar radiation pressure of element
$\vec{M}_{S_{Logic}}$ Logic gate used by 42 to calculate moments due to solar radiation pressure of element

Frame Transformations

$H_{eci/fm}$ Direction cosine matrix of FM frame with respect to ECI frame
$H_{ecr/eci}$ Direction cosine matrix of ECI frame with respect to ECR frame
$H_{eme/eci}$ Direction cosine matrix of ECI frame with respect to J2000 frame

Forces, Moments, and Gravity

$\vec{F}_S$ Force due to solar radiation pressure
$\vec{F}_a$ Force due to absorbed radiation
$\vec{F}_r$ Force due to specular reflection
$\vec{F}_d$ Force due to diffusive reflection
$\vec{M}_S$ Moment due to solar radiation pressure
$\vec{M}_g$ Moment due to gravitational gradient
$\vec{M}_{fm}$ Moment in FM frame
ℓ Degree of spherical harmonic
m Order of spherical harmonic
V Gravitational potential
∇V Gradient of gravitational potential
a_e Semi-major axis of the Earth's reference ellipsoid
$P_{\ell,m}$ Associated Legendre of gravitational potential and is a function of $\sin(\phi)$
ϕ_E Degree latitude in radians
λ_E Degree longitude in radians
$C_{\ell,m}$ Cosine coefficient of gravitational potential
$S_{\ell,m}$ Sine coefficient of gravitational potential
μ_E Earth gravitational constant
μ_S Sun gravitational constant
μ_M Moon gravitational constant

Vehicle Properties

$\hat{n}$ Unit vector formal to the vehicle's body
A Vehicle surface area
C_a Absorbed radiation coefficient
C_{sr} Specular reflection coefficient
C_{dr} Diffusive reflection coefficient
$\vec{r}_p$ Parametrized vector that denotes the vehicle's surface integration domain and is a function of u and v.
u Radius length of surface integration
v Angle of surface integration
R_n Vehicle nose radius
R_c Vehicle cone radius
δ, δ_c Vehicle half-cone angle
$X_{cent.}$ Centroid along x-axis of vehicle geometry
$\vec{r}_{cone_{cent.}}$ Centroid position vector of conical frustrum segment in local frame
$\vec{r}_{sphere_{cent.}}$ Centroid position vector of spherical segment in local frame
$\vec{r}_{perfect\ sphere_{cent.}}$ Centroid position vector of sphere in local frame
$\vec{r}_{cone_{cent.\to cg}}$ Centroid position vector of conical frustrum segment in Body frame with respect to vehicle nose
$\vec{r}_{sphere_{cent.\to cg}}$ Centroid position vector of spherical segment in Body frame with respect to vehicle nose

$\vec{r}_{Perfect\ Sphere_{cent.\rightarrow cg}}$	Centroid position vector of sphere in Body frame with respect to vehicle nose
Xcg	Position of center of gravity x-axis in Body frame
Ycg	Position of center of gravity y-axis in Body frame
Zcg	Position of center of gravity z-axis in Body frame
M	Vehicle mass
I_{xx}	Vehicle mass moment of inertia about the Body frame x-axis
I_{yy}	Vehicle mass moment of inertia about the Body frame y-axis
I_{zz}	Vehicle mass moment of inertia about the Body frame z-axis
I_{xy}	Vehicle mass product of inertia, Body x and y axes
I_{xz}	Vehicle mass product of inertia, Body x and z axes
I_{yz}	Vehicle mass product of inertia, Body y and z axes
I	Inertia Tensor

Table of Contents

Page

ABSTRACT ..... *iii*

NOMENCLATURE ..... *iv*

LIST OF FIGURES ..... *x*

LIST OF GRAPHS ..... *xi*

INTRODUCTION *1*

Mars Sample Return Overview 1

DESCRIPTION OF FRAMES *4*

EES Body Frame 4

EES Flight Mechanic (FM) Frame 4

Earth's Mean Equator and Equinox 2000 (EME 2000) 5

Earth Centered Inertial (ECI) 6

Earth Centered Rotating (ECR) 6

MODELING AND SIMULATION *7*

Solar Radiation Pressure 8

Method I (42) 11

Method II (POST2 Generalized Sphere-cone) 13

Method III (POST2 Generalized Sphere) 18

Gravitational Spherical Harmonics 20

3rd Body Perturbations 22

Gravity Gradient Torque 22

EQUATIONS OF MOTION *24*

Frame Transformations 24

Translational Acceleration (FM Frame) 24

Angular Accelerations (FM Frame) 25

RESULTS *26*

42 vs. POST2 (No SRP Forces and Moments) 26

42 (SRP Method I) vs. POST2 (SRP Method II) 29

42 (SRP Method I) vs. POST2 (SRP Method III) 35

CONCLUSION *41*

Future Work 41

REFERENCES *43*

APPENDIX 1: POST2 Simulation Inputs *44*

Vehicle Properties 44
Initial Vehicle States 45
Planetary Constants 45
Miscellaneous Constants 45
Gravitational Harmonic Coefficients 46
APPENDIX 2: 42 vs. MONTE Comparisons *51*
Plots of Relative Difference 51
42 vs. MONTE Summary Table 53

LIST OF TABLES

Page

Table 1: Conical Frustum Centroid 16
Table 2: 42 vs. POST2 Summary (SRP Off) 28
Table 3: 42 vs. POST2 Summary (Method I vs. Method II) 34
Table 4: 42 vs. POST2 Summary (Method I vs. Method III) 40
Table 5: Vehicle Properties 44
Table 6: EES Initial States 45
Table 7: Planetary Constants 45
Table 8: Misc. Constants 45
Table 9: Gravitational Harmonic Coefficients 50

LIST OF FIGURES

Page
Figure 1: Mars Sample Return Campaign Elements 3
Figure 2: EES Flight Mechanic and Body Frame 4
Figure 3: EME 2000 Frame 5
Figure 4: Earth Centered Inertial Frame 6
Figure 5: AEDL Phase of CCRS 8
Figure 6: Components of SRP Forces acting on a Flat Plate 9
Figure 7: EES Grid Side View 12
Figure 8: EES Grid Aft View 12
Figure 9: Previous NASA Sphere-Cone Designs 13
Figure 10: EES Sphere-cone Geometry 14
Figure 11: EES Conical Frustum 15
Figure 12: EES Sphere 17
Figure 13: EES Perfect Sphere Approximation 19

LIST OF GRAPHS

Page
Graph 1: Position Difference (42 vs. POST2) 26
Graph 2: Velocity Difference (42 vs. POST2) 26
Graph 3: Euler Angle Differences (42 vs. POST2) 27
Graph 4: Euler Rate Differences (42 vs. POST2) 27
Graph 5:SRP Forces (Method I vs. Method II) 29
Graph 6: SRP Moments (Method I vs. Method II) 29
Graph 7: Position Difference (Method I vs. Method II) 30
Graph 8: Velocity Difference (Method I vs. Method II) 30
Graph 9: Yaw Difference (Method I vs. Method II) 31
Graph 10: Yaw Rate Difference (Method I vs. Method II) 31
Graph 11: Pitch Difference (Method I vs. Method II) 32
Graph 12: Pitch Rate Difference (Method I vs. Method II) 32
Graph 13: Roll Difference (Method I vs. Method II) 33
Graph 14: Roll Rate Difference (Method I vs. Method II) 33
Graph 15: SRP Forces (Method I vs. Method III) 35
Graph 16: SRP Moments (Method I vs. Method III) 35
Graph 17:Position Difference (Method I vs. Method III) 36
Graph 18: Velocity Difference (Method I vs. Method III) 36
Graph 19: Yaw Difference (Method I vs. Method III) 37
Graph 20: Yaw Rate Difference (Method I vs. Method III) 37
Graph 21: Pitch Difference (Method I vs. Method III) 38
Graph 22: Pitch Rate Difference (Method I vs. Method III) 38
Graph 23: Roll Difference (Method I vs. Method III) 39
Graph 24: Roll Rate Difference (Method I vs. Method III) 39

INTRODUCTION

Solar radiation pressure (SRP) is a force that acts on a body due to the momentum transfer of electromagnetic waves. Forces caused by SRP are the second most dominant force acting on a body during passive exoatmospheric flight, the first being gravitational fields. Although these forces are relatively small compared to gravity, the forces and moments caused by SRP can impact the position, velocity, and orientation of an unpowered vehicle over significant amounts of time. The two objectives of this project are to conduct a comparative study of two state-of-the-art codes, 42 and Program to Optimize Simulated Trajectories II (POST2), with and without their respective applications of SRP forces and moments. This involves having to develop a generalized project module that can be integrated into POST2 that models SRP forces and moments acting on a vehicle/satellite.

The motivation of this project came as part of the work being done in support of NASA's mission, Mars Sample Return (MSR). MSR is a joint mission between NASA, the European Space Agency, and other industries that aim to bring Martian samples back to Earth. Several trajectory simulation tools are used to model exoatmospheric and atmospheric phases of flight. 42 and MONTE have been used to produce independent results of exoatomospheric phases of flight while POST2 and DESCENDS have been primarily used to model atmospheric phases.

Mars Sample Return Overview

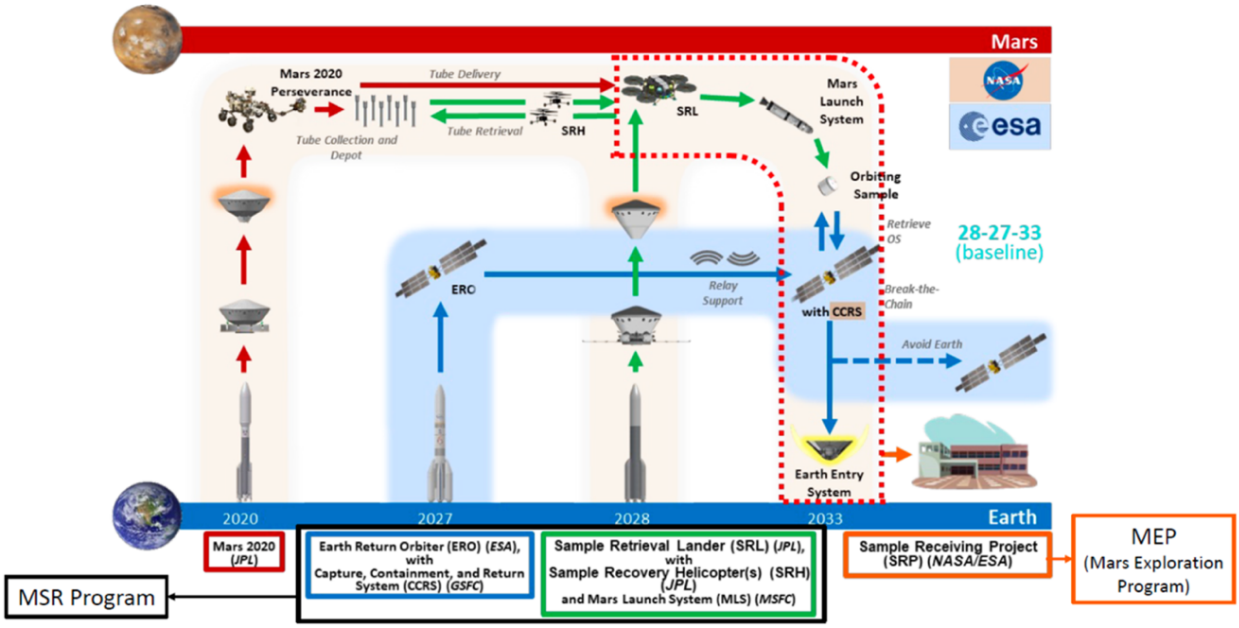
The campaign elements of MSR are illustrated in figure (1) and described in detail in [1]. The first phase is currently being accomplished by the Perseverance rover which landed on Mars in 2021 and began collecting samples taken from the surface. The MSR program represents the second and third phases of the campaign which involves landing a sample retrieval vehicle on

Mars to launch the samples into Mars orbit and sending an orbiter to intercept and return the orbiting samples to Earth (ERO). The fourth phase of the campaign is part of the Sample Receiving Program which aims to analyze the returned samples under protective measures.

The primary payload of ERO is the Capture, Containment, and Return System (CCRS). The purpose of CCRS is to capture the orbital sample upon rendezvous with ERO and is described in [2]. CCRS will then capture and contain the orbital sample and insert the sample into the Earth Entry System (EES). Approximately three days prior to Earth atmospheric entry, EES would be ejected from ERO and carry the samples through Earth's atmosphere and land on the Utah Test and Training Grounds (UTTR).

However, as part of the NASA response to the recent MSR Independent Review Board's report, and the current budget environment, the MSR Program is undergoing a consideration of changes in its mission architecture. This document is based upon the previous MSR architecture in which CCRS would return the Martian samples to Earth. The CCRS project completed system development to a Preliminary Design Review level of maturity in mid-December 2023, after which the project was stopped indefinitely pending the results of the re-architecting effort. The decision to implement MSR will not be finalized until NASA's completion of the National

Environmental Policy Act process. This document is being made available for information purposes only.



Source: NASA

Figure 1: Mars Sample Return Campaign Elements

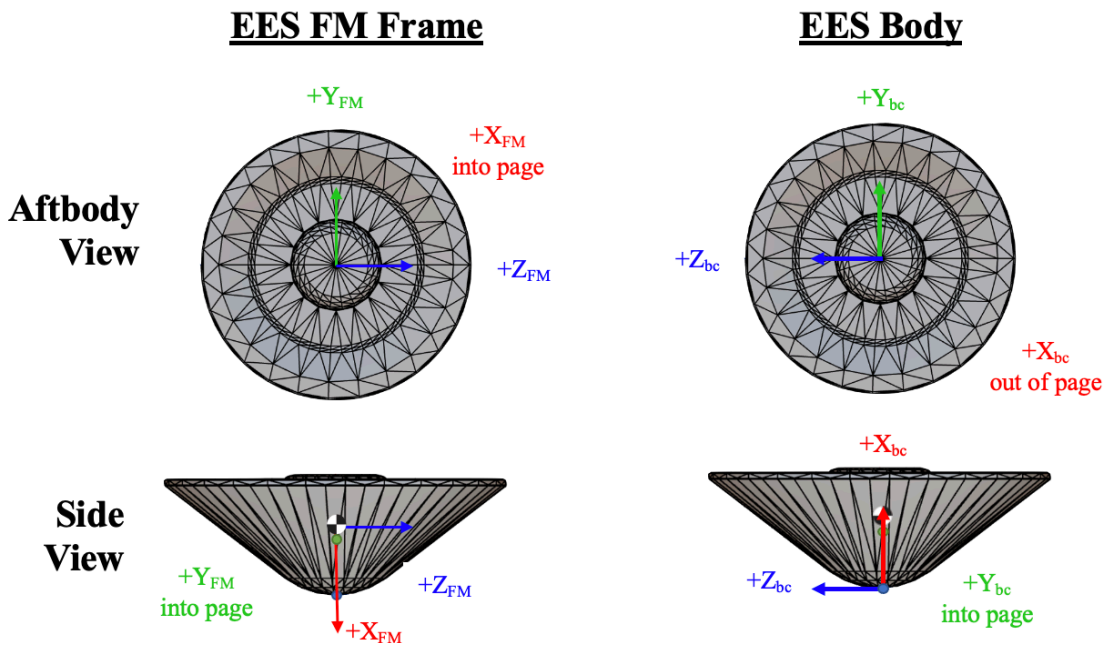
DESCRIPTION OF FRAMES

EES Body Frame

The body frame is a structural frame in which the center of gravity and other mass properties are defined. In the case of EES, the origin of the body frame is placed at the nose of the vehicle, $+X_{bc}$ points inwards towards the vehicle, $-Y_{bc}$ is aligned with a bracket that attaches EES to ERO while Z_{bc} completes the right-hand frame. The body frame can be seen depicted in figure (2).

EES Flight Mechanic (FM) Frame

The flight mechanic frame is defined with its origin collocated at the center of gravity. The $+X_{FM}$ and $+Z_{FM}$ are oriented anti-parallel to $+X_{bc}$ and $+Z_{bc}$ respectfully and Y_{FM} completes the right-hand frame. The flight mechanic frame can be seen depicted in figure (2).

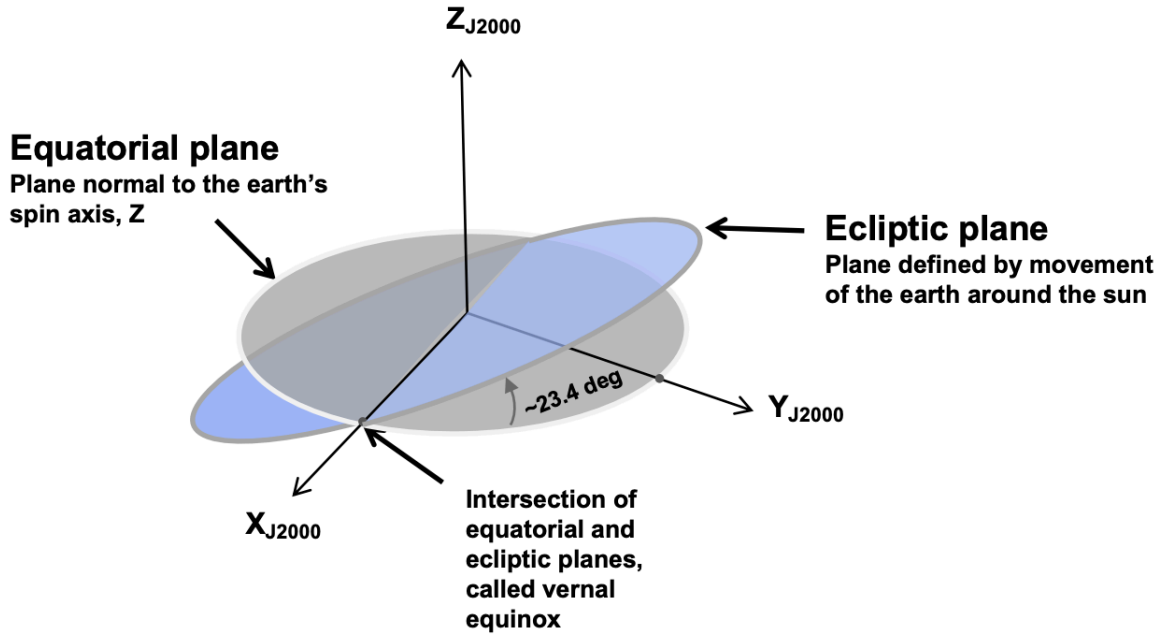


Source: NASA

Figure 2: EES Flight Mechanic and Body Frame

Earth's Mean Equator and Equinox 2000 (EME 2000)

EME 2000 is an inertial reference frame specified by the orientation of the Earth's mean equator and equinox at a particular epoch known as the J2000 epoch. The J2000 epoch corresponds to Greenwich noon on January 1, 2000 Barycentric Dynamical Time. In this frame $+X_{J2000}$ intersects Earth's equatorial plane and ecliptic plane, $+Z_{J2000}$ points towards Earth's geographic north pole and is normal to the equatorial plane, and Y_{J2000} completes the rand-hand frame. This frame describes the states of EES relative to celestial bodies (e.g. Sun, Earth and Moon). The EME 2000 frame can be seen depicted in figure (3).

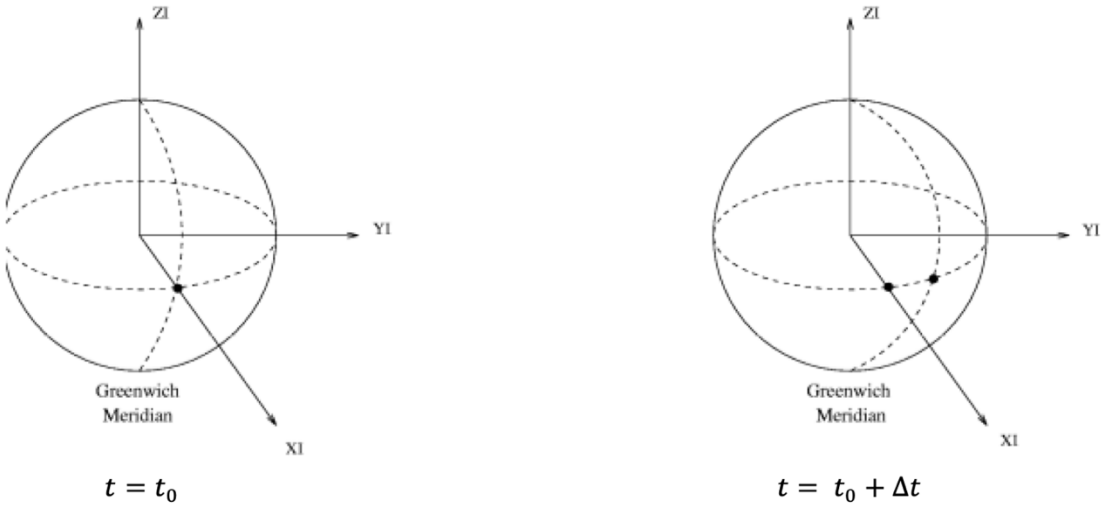


Source: Jet Propulsion Laboratory

Figure 3: EME 2000 Frame

Earth Centered Inertial (ECI)

The origin of the ECI frame stays fixed at the Earth's center as it moves through space. The $+X_I$ points in the direction of the Greenwich meridian at the simulation's initial epoch, $+Z_I$ points towards the geographic north pole, and Y_I completes the right-hand frame. The ECI frame can be seen depicted in figure (4).



Source: NASA

Figure 4: Earth Centered Inertial Frame

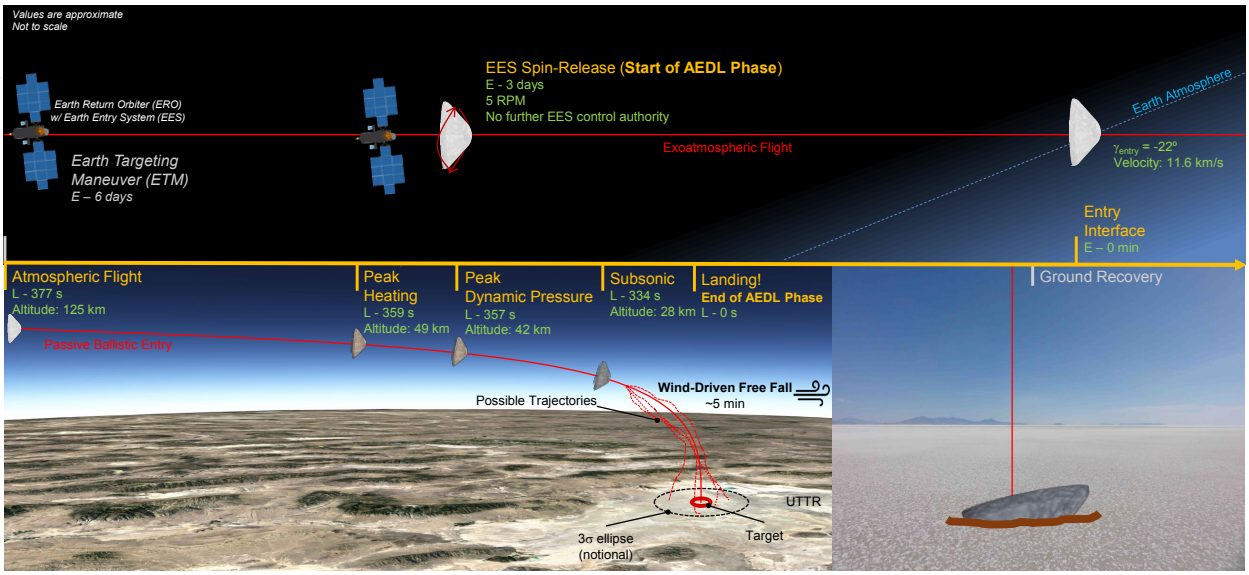
Earth Centered Rotating (ECR)

The ECR frame has the same convention as the ECI frame except rotates with the Earth about the z-axis after the initial epoch.

MODELING AND SIMULATION

The Approach, Entry, Decent, and Landing (AEDL) phase of MSR's CCRS begins three days prior to EES's entry into Earth's atmosphere. ERO would eject EES as it begins its 72-hour passive trajectory towards Earth. After atmospheric interface, EES will descend through Earth's atmosphere where it would land safely at UTTR. The concept of operations is illustrated in figure (5).

Thus far 42 has been the primary 6 degrees of freedom trajectory tool to model the 72-hour period of exoatmospheric flight while MONTE has been used to compare independent results. Similarly, DSENDS has been used to compare trajectory solutions with POST2 during atmospheric entry, descent, and landing. As the project matures, it is desirable to utilize one trajectory tool as the primary simulation to model the exoatmospheric and atmospheric phases of AEDL. This section addresses the different methodologies of modeling SRP forces and moments in POST2, along with the other forces and moments being modeled in POST2 and 42 during EES's exoatmospheric phase of flight.



Source: NASA/Jet Propulsion Lab

Figure 5: AEDL Phase of CCRS

Solar Radiation Pressure

The implementation of SRP forces and moments in both 42 and POST2 vary and is proportional to the level of effort and computation required to model the 72-hour period SRP forces and moments acting on EES prior to atmospheric interface. In this section we will explore the 42 implementation of modeling SRP forces and moments along with the two generalized implementations created for POST2.

SRP forces are a function of the satellite's geometry, solar angles of incidence, the distance of the satellite with respect to the Sun, and the satellite's material properties. SRP forces are the resultant of three separate forces and their respective coefficients as shown in Eq. (1) and illustrated in figure (6). In figure (6), $\hat{n}$ is the unit vector normal to the body, $\hat{S}$ is the solar unit vector of the satellite with respect to the Sun, and β is the angle between the solar unit vector and unit vector normal to the satellite's body.

These forces are caused by the absorbed radiation, specular and diffusive reflection. The forces and moments due to SRP can be derived analytically by following the methodology in [3] by assuming the surfaces of EES behave as a black body, perfect mirror, and a Lambert diffuser. With these assumptions the absorption, specular reflection and diffusive reflection coefficients are independent of the solar incidence angle, direction, and wavelength and can be treated as constant.

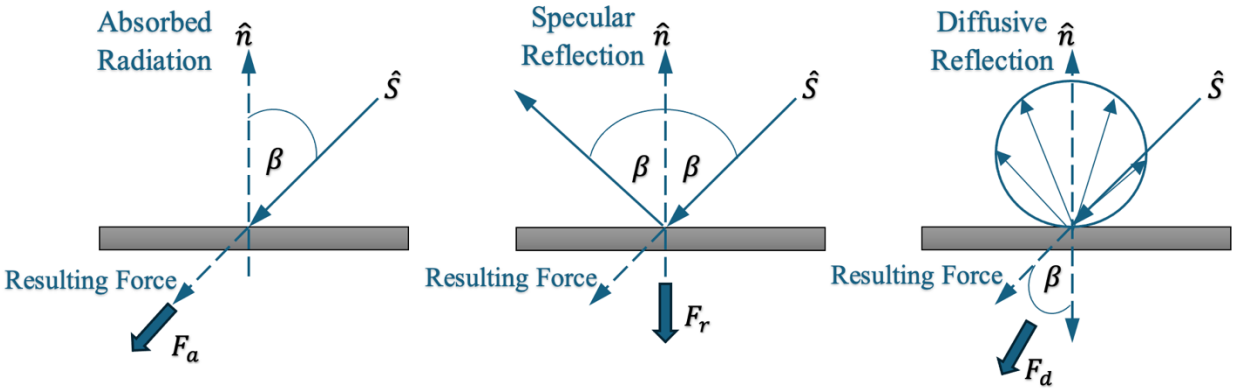


Figure 6: Components of SRP Forces acting on a Flat Plate

$$d\vec{F}_S = d\vec{F}_a + d\vec{F}_r + d\vec{F}_d \tag{1}$$

$$d\vec{F}_a = -P_S C_a (\hat{S} \cdot \hat{n})(\hat{S}) dA \tag{2}$$

$$d\vec{F}_r = -2P_S C_{sr} (\hat{S} \cdot \hat{n})^2 (\hat{n}) dA \tag{3}$$

$$d\vec{F}_d = -P_S C_{dr} (\hat{S} \cdot \hat{n})^2 (\hat{S} \cdot \frac{2}{3}\hat{n}) dA \tag{4}$$

$$C_a + C_{sr} + C_{dr} = 1 \tag{5}$$

$$\hat{S} \cdot \hat{n} = \cos(\beta) \tag{6}$$

$$P_s = \frac{\phi_s}{c} \tag{7}$$

Here in Eq. (7), P_S is equivalent to the quotient of the solar heat flux (ϕ_s) and speed of light (c).

$$\phi_s = k_{1AU} \frac{(1\ AU)^2}{\|\vec{r}_{Sun \rightarrow Sat.}\|^2} \tag{8}$$

The solar heat flux on a satellite is dependent on its distance from the Sun. A good approximation of the solar heat flux involves using the solar heat flux observed at one astronomical unit (k_{1AU}) and the inverse-square law. Here in Eq. (8), $\vec{r}_{Sun \rightarrow Sat.}$ is the position vector of the satellite with respect to the Sun.

$$d\vec{F}_S = -\frac{\phi_s}{c}\left[2\left(\frac{C_{dr}}{3}\cos(\beta) + C_{sr}cos^2(\beta)\right)\hat{n} + (1 - C_{sr})\cos(\beta)\hat{S}\right]dA \tag{9}$$

Using the relationships in Eqs. (2-8) and substituting them into Eq. (1) yields the final integrand seen in Eq. (9).

$$\vec{n} = \frac{\partial \vec{r}_p(u,v)}{\partial u} \times \frac{\partial \vec{r}_p(u,v)}{\partial v} \tag{10}$$

The normal vector can be calculated as the cross product of the partials of $\vec{r}_p$. Here $\vec{r}_p$ is a parametric vector that describes the domain of surface integration across the satellite and is a function of the radius length (u) and angle (v).

$$\hat{n} = \frac{\vec{n}}{\|n\|} \tag{11}$$

$$\hat{S} = \hat{r}_{Sun \rightarrow Sat.} = [\cos(\alpha)\cos(\beta) \quad \sin(\beta) \quad \sin(\alpha)\cos(\beta)] \tag{12}$$

The solar unit vector is equivalent to the position unit vector of the satellite with respect to the Sun. The components of the solar unit vector are a function of the angles β and α, which are analogous to the sideslip angle and angle of attack often described in aerodynamics.

$$\vec{F}_S = -\frac{\phi_s}{c}\iint_{u_0\,v_0}^{u_1\,v_1}\left[2\left(\frac{C_{dr}}{3}\cos(\beta)+C_{sr}cos^2(\beta)\right)\hat{n}+(1-C_{sr})\cos(\beta)\hat{S}\right]dA \quad (13)$$

$$\vec{M}_S = -\frac{\phi_s}{c}\iint_{u_0\,v_0}^{u_1\,v_1}\vec{r}\times\left[2\left(\frac{C_{dr}}{3}\cos(\beta)+C_{sr}cos^2(\beta)\right)\hat{n}+(1-C_{sr})\cos(\beta)\hat{S}\right]dA \quad (14)$$

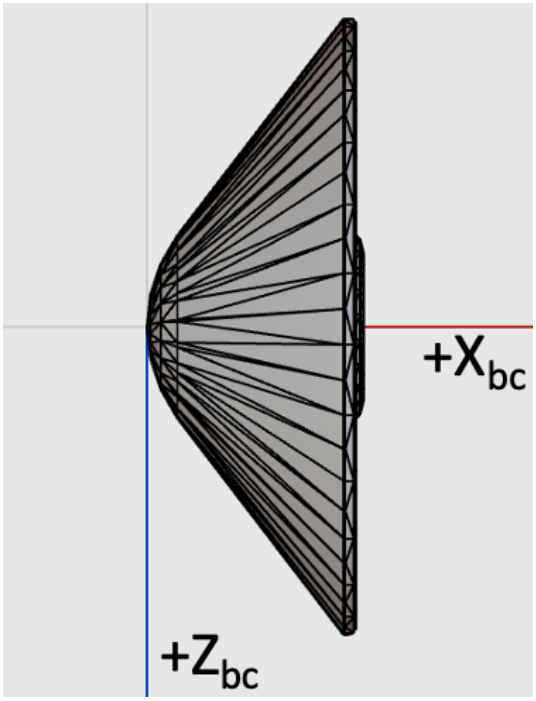
Eq. (14) shows that the moment caused by SRP is equivalent to the cross product of the position vector of the satellite's moment arm ($\vec{r}$) and the integrand of Eq. (9).

Method I (42)

The SRP model implemented by 42 takes the outer mold line (OML) of EES and creates a grid of 1362 distinct faces with a particular area, normal direction, and geometric center. A depiction of the grided faces can be seen in figures (7-8). At each timestep during the simulation, 42 determines which polygons are in the flow of solar radiation by using a Boolean logic summarized in Eq. (15), and if true, applies the formula of SRP forces shown in Eq. (13) and moments in Eq. (14) to the polygon. The vector sum of 1362 faces are then computed to produce a resultant SRP force and moment imposed on EES.

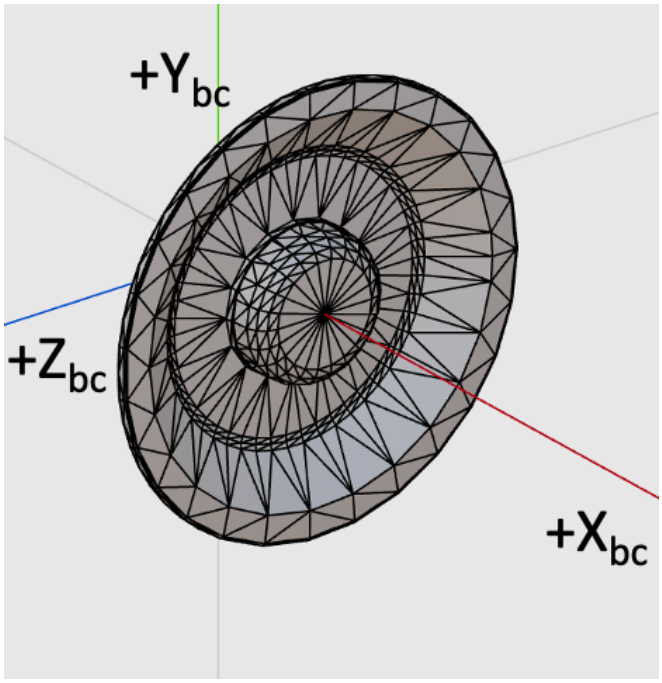
Of the three methods of modeling SRP in this section, this method offers the highest fidelity. However, this method takes considerable amount of effort to create the OML grid, is specific only to EES's geometry, and requires more computational resources to account for all the forces and moments imposed on 1362 distinct faces.

$$\vec{F}_{S_{Logic}}, \vec{M}_{S_{Logic}} = \begin{cases} 1, & \cos(\beta) < 0 \\ 0, & \cos(\beta) \geq 0 \end{cases} \quad (15)$$



Source: NASA

Figure 7: EES Grid Side View



Source: NASA

Figure 8: EES Grid Aft View

Method II (POST2 Generalized Sphere-cone)

The sphere-cone design is one often used for vehicle's designed for atmospheric interface. Over the past two decades, NASA missions such as Genesis, Stardust, OSIRIS-Rex, and MSR have all utilized sphere-cone designs. Given how often sphere-cone geometries are utilized, it is useful to develop a more generalized method of SRP modeling. This method can be achieved by partitioning the sphere-cone into a conical frustum and spherical geometry.



Source: NASA

Figure 9: Previous NASA Sphere-Cone Designs

The sphere-cone geometry can be parametrized in terms of the vehicle's nose radius (R_n), cone radius (R_c), and half-cone angle (δ). Figure (10) illustrates the parametrization of the sphere-cone geometry. To simplify the domain of integration, it is useful to partition and parametrize the geometry into spherical and conical frustum segments.

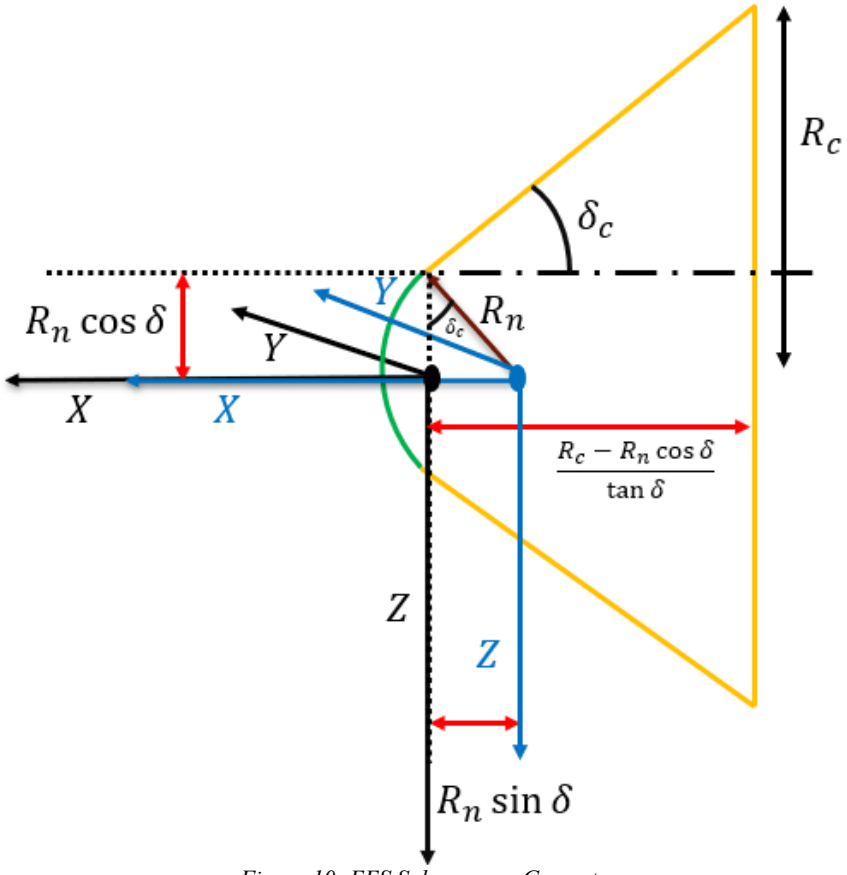


Figure 10: EES Sphere-cone Geometry

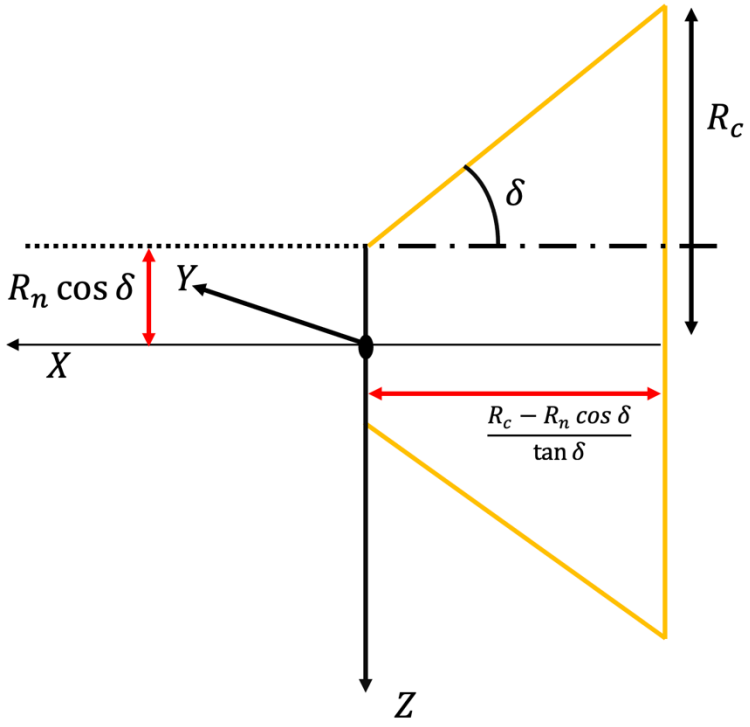


Figure 11: EES Conical Frustum

$$r_{p_{Cone}} = \left[-\frac{u}{\tan(\delta)}, \quad u\cos(v), \quad -u\sin(v)\right] \qquad u \in [R_n\cos(\delta),\ R_c], v \in [0, 2\pi] \tag{16}$$

It is assumed that SRP distributed evenly across the body causing the sum of SRP forces to act on the geometry's centroid. Due to EES's axisymmetric geometry, we simply need to calculate the centroid located on the local x-axis. In the case of the conical frustum, we can determine the centroid by partitioning the shape into a rectangle of with dimensions $\frac{R_c - R_n\cos(\delta)}{\tan(\delta)} \times R_n\cos(\delta)$ and a right triangle with dimensions $\frac{R_c - R_n\cos(\delta)}{\tan(\delta)} \times R_c - R_n\cos(\delta)$.

	Area	$\overline{x}$	$\overline{x}A$
Rectangle	$\frac{(R_c - R_n\cos(\delta))R_n\cos(\delta)}{\tan(\delta)}$	$\frac{R_c - R_n\cos(\delta)}{2\tan(\delta)}$	$\frac{(R_c - R_n\cos(\delta))^2 R_n\cos(\delta)}{2\tan^2(\delta)}$
Triangle	$\frac{(R_c - R_n\cos(\delta))^2}{2\tan(\delta)}$	$\frac{2(R_c - R_n\cos(\delta))}{3\tan(\delta)}$	$\frac{(R_c - R_n\cos(\delta))^3}{3\tan^2(\delta)}$
Total	$\frac{(R_c - R_n\cos(\delta))}{\tan(\delta)}\left(R_n\cos(\delta) + \frac{R_c - R_n\cos(\delta)}{2}\right)$		$\frac{(R_c - R_n\cos(\delta))^2}{2\tan^2(\delta)}\left(R_n\cos(\delta) + \frac{2(R_c - R_n\cos(\delta))}{3}\right)$

Table 1: Conical Frustum Centroid

$$X_{cent.} = \frac{\Sigma\overline{x}A}{\Sigma\text{Area}} = \frac{(R_c - R_n\cos(\delta))(2(R_c - R_n\cos(\delta)) + 3R_n\cos(\delta))}{3\tan(\delta)(R_c - R_n\cos(\delta) + 2R_n\cos(\delta))} \quad (17)$$

$$\vec{r}_{cone_{cent.}} = [X_{cent.}, \quad 0, \quad 0] \quad (18)$$

$$\vec{r}_{cone_{cent.\to cg}} = [Xcg - (X_{cent.} + R_n - R_n\sin(\delta)), \quad Ycg, \quad Zcg] \quad (19)$$

Here in Eq. (19), Xcg, Ycg, and Zcg are the components of the center of gravity position relative to the satellite's nose. We must also account for the distance between the nose and the start of the conical frustum, $R_n - R_n\sin(\delta)$, to get the complete position vector of the frustum's centroid with respect to the nose. The domain of the conical frustum parameterized in Eq. (16) and the moment arm in Eq. (19) can now be used to calculate the SRP forces and moments of the conical frustum segment by following the process in Eqs. (10-14).

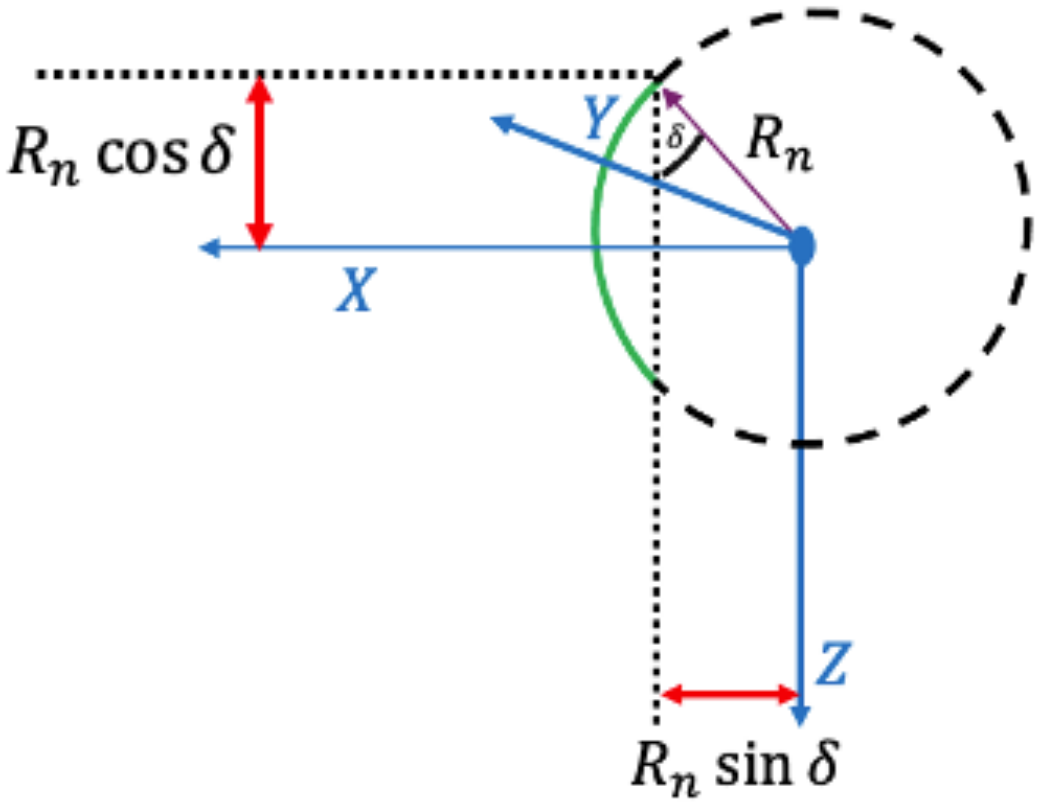


Figure 12: EES Sphere

Here we are concerned only with the green highlighted section as seen in figure (12) when parametrizing the spherical portion of the satellite's geometry. The centroid of the spherical section can be approximated by treating the area as a semielliptical shape with semi-major axis equal to $R_n\cos(\delta)$ and semi-minor axis equal to $R_n - R_n\sin(\delta)$.

$$r_{p_{Sphere}} = \left[u\,,\quad \sqrt{{R_n}^2 - u^2}\,\cos(v)\,,\quad -\sqrt{{R_n}^2 - u^2}\,\sin(v)\right]\; u \in [R_n\sin(\delta),\, R_n]\,, v \in [0, 2\pi] \tag{20}$$

$$\vec{r}_{sphere_{cent.}} = \left[\frac{4\left(R_n - R_n\sin(\delta)\right)}{3}\,,\quad 0\,,\quad 0\right] \tag{21}$$

$$\vec{r}_{sphere_{cent.\to cg}} = \left[Xcg - \frac{4\left(R_n - R_n\sin(\delta)\right)}{3}\,,\quad Ycg\,,\quad Zcg\right]$$

(22)

The domain of the conical frustum parameterized in Eq. (20) and the moment arm in Eq. (22) can now be used to calculate the SRP forces and moments of the spherical segment by following the process in Eqs. (10-14). Eq. (23) shows the vector sum of the SRP forces and moments utilizing the generalized sphere-cone method.

$$\vec{F}_S = \vec{F}_{S_{cone}} + \vec{F}_{S_{sphere}}$$

$$\vec{M}_S = \vec{M}_{S_{cone}} + \vec{M}_{S_{sphere}}$$

(23)

Method III (POST2 Generalized Sphere)

The third method implemented into POST2 is the most generalized of the three methods used to calculate the SRP forces in moments. This method simply approximates the satellite as a perfect sphere with radius R_c. This method provides the least amount of fidelity but removes the trouble of complicated parametrization and centroid calculations described in Method II.

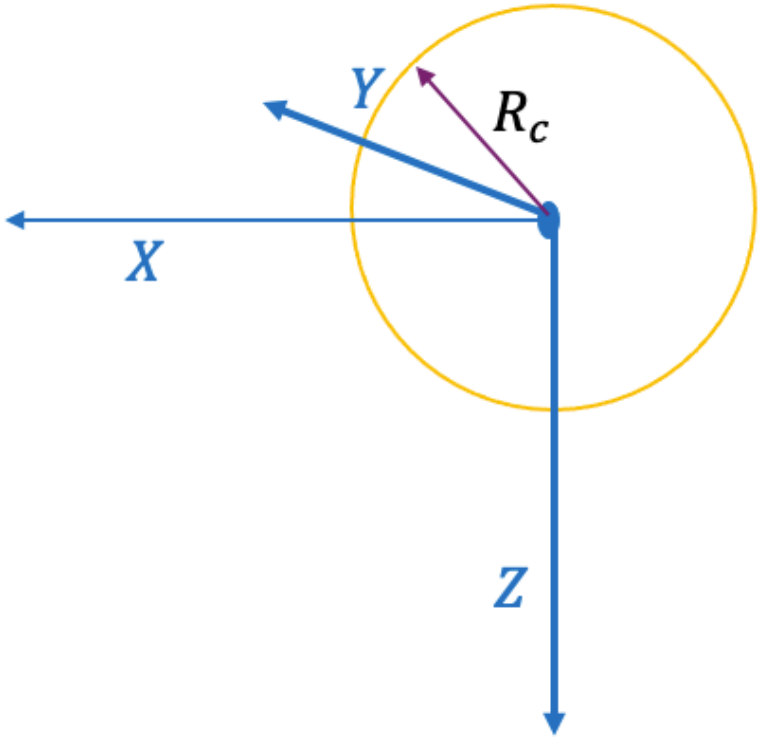


Figure 13: EES Perfect Sphere Approximation

$$r_{p_{Perfect\ Sphere}} = [-u\,,\quad -u\cos(v)\,,\quad u\sin(v)] \qquad u \in [0,\ R_c]\,, v \in [0, 2\pi] \tag{24}$$

$$\vec{r}_{Perfect\ Sphere_{cent.}} = [R_c\,,\quad 0\,,\quad 0] \tag{25}$$

$$\vec{r}_{Perfect\ Sphere_{cent.\to cg}} = [Xcg - R_c\ ,\quad Ycg\,,\quad Zcg] \tag{26}$$

The domain of the sphere parameterized in Eq. (24) and the moment arm in Eq. (26) can now be used to calculate the SRP forces and moments of the sphere by following the process in Eqs. (10-14). Sample MATLAB code that solves for SRP forces for Method II and Method III described in this section is found in Appendix 2.

Gravitational Spherical Harmonics

Satellites affected by Earth's gravitational field experience a spectrum of perturbations due to Earth's oblateness and non-uniform density. The perturbations produced on a satellite can be captured using Kaula's analytical expressions described in [4]. For comparison purposes, 42 and POST2 used a gravitational field of 18 degrees (ℓ) and 18 order (m) in their respective simulations.

$$V = \frac{\mu_E}{r_{E\to Sat.}} \sum_{\ell=0}^{\infty} \left(\frac{a_e}{r_{E\to Sat.}}\right)^{\ell} \sum_{m=0}^{\ell} P_{\ell,m}(\sin(\phi_E)) \left[C_{\ell,m} \cos(m\,\lambda_E) + S_{\ell,m} \sin(m\,\lambda_E)\right] \tag{27}$$

$$P_{\ell,m}(\sin(\phi_E)) = \frac{(1 - sin^2(\phi_E))^{m/2}}{2^{\ell}} \sum_{k=0}^{\frac{\ell-m}{2}} (-1)^k \frac{(2\ell - 2k)!}{k!\,(\ell - k)!\,(\ell - m - 2k)} \sin(\phi)^{\ell-m-2k} \tag{28}$$

Here in Eq. (27), the gravitational potential (V) can be calculated as a function of the field's degree (ℓ), order (m), Earth's gravitational constant (μ_E), the geocentric radius of the satellite with respect to the Earth ($r_{E\to Sat.}$), semi-major axis of the Earth's reference ellipsoid (a_e), the Associated Legendre Function ($P_{\ell,m}$) of degree ℓ and order m, the coefficients $C_{\ell,m}$ and $S_{\ell,m}$, and the satellite's latitude (ϕ_E) and longitude (λ_E) in the ECR frame. The general form of the Associated Legendre can be seen in Eq. (28). The $C_{\ell,m}$ and $S_{\ell,m}$ coefficients used in the POST2 simulation are sourced from [5] and can be referenced in Appendix 1.

The representation of Eq. (27) can be thought of three components depicted in Eq. (29). The V_0 term corresponds to the degree and order zero term, where $P_{0,0}$ and $C_{0,0}$ are equal to 1. Substituting $P_{0,0}$ and $C_{0,0}$ into Eq. (27) results in the term that treats the Earth as a point mass. The V_1 term are those terms that do not have a longitudinal dependency. These are the terms that occur when $\ell \geq 1$ and $m = 0$. Lastly V_2 represents the terms with longitudinal dependencies.

$$V = V_0 + V_1 + V_2 \tag{29}$$

$$V_0 = \frac{\mu_E}{r_{E\to Sat.}} \tag{30}$$

$$V_1 = \frac{\mu_E}{r_{E\to Sat.}} \sum_{\ell=1}^{\infty} \left(\frac{a_e}{r_{E\to Sat.}}\right)^{\ell} P_{\ell,0}(\sin(\phi_E)) C_{\ell,0} \tag{31}$$

$$V_2 = \frac{\mu_E}{r_{E\to Sat.}} \sum_{\ell=1}^{\infty} \left(\frac{a_e}{r_{E\to Sat.}}\right)^{\ell} \sum_{m=1}^{\ell} P_{\ell,m}(\sin(\phi_E)) \left[C_{\ell,m} \cos(m\,\lambda_E) + S_{\ell,m} \sin(m\,\lambda_E)\right] \tag{32}$$

The gravitational accelerations from the spherical harmonic model can be obtained by the gradient of Eq. (27). The general form of the gravitational acceleration produced by spherical harmonics is expressed in Eqs. (33) and (34). Here the components of $\vec{a}_g$ are expressed in the ECR frame via a spherical coordinate system where $\hat{r}_{E\to Sat.}$ points along the radius of the satellite with respect to the Earth's center, $\hat{\phi}$ is in the increasing north latitude and $\hat{\lambda}$ is in the direction of increasing eastward longitude. POST2 calculates $\vec{a}_g$ with respect to the ECR frame.

$$\vec{a}_g = \nabla V = \frac{\partial V}{\partial r} \hat{r}_{E\to Sat.} + \frac{1}{r} \frac{\partial V}{\partial \phi_E} \hat{\phi} + \frac{1}{r \cos(\phi)} \frac{\partial V}{\partial \lambda_E} \hat{\lambda} \tag{33}$$

$$\vec{a}_g = \left\{ -\frac{\mu_E}{{r_{E\to Sat.}}^2} \sum_{\ell=0}^{\infty} (\ell+1) \left(\frac{a_e}{r_{E\to Sat.}}\right)^{\ell} \sum_{m=0}^{\ell} P_{\ell,m}\left(\sin(\phi_E)\right)\left[C_{\ell,m}\cos(m\,\lambda_E) + S_{\ell,m}\sin(m\,\lambda_E)\right] \right\} \hat{r}_{E\to Sat.}$$

$$+ \left\{ \frac{\mu_E}{{r_{E\to Sat.}}^2} \sum_{\ell=1}^{\infty} \left(\frac{a_e}{r_{E\to Sat.}}\right)^{\ell} \sum_{m=0}^{\ell} \frac{\partial P_{\ell,m}\left(\sin(\phi_E)\right)}{\partial \phi_E} \left[C_{\ell,m}\cos(m\,\lambda_E) + S_{\ell,m}\sin(m\,\lambda_E)\right] \right\} \hat{\phi}$$

$$+ \left\{ \frac{\mu_E}{{r_{E\to Sat.}}^2} \sum_{\ell=1}^{\infty} \left(\frac{a_e}{r_{E\to Sat.}}\right)^{\ell} \sum_{m=1}^{\ell} m \frac{P_{\ell,m}\left(\sin(\phi_E)\right)}{\cos(\phi_E)} \left[-C_{\ell,m}\sin(m\,\lambda_E) + S_{\ell,m}\cos(m\,\lambda_E)\right] \right\} \hat{\lambda}$$

(34)

3rd Body Perturbations

The 3rd body perturbations are perturbations caused by the gravitational influence of other celestial bodies other than the central body (e.g. Earth). The POST2 simulation considers the gravitational perturbations contributed by the Sun and Earth's moon. The Cowell Method described in [6] is used by POST2 to account for these additional gravitational accelerations. Here in Eq. (35), μ_M and μ_S are the gravitational constants for the Moon and Sun respectively while $\vec{r}_{E\to Sat.}$, $\vec{r}_{S\to Sat.}$, $\vec{r}_{M\to Sat.}$ are the positions vectors of the satellite with respect to the Earth, Sun, and Moon respectively. POST2 calculates $\vec{a}_{3B}$ with respect to the EME 2000 frame.

$$\vec{a}_{3B} = -\mu_M \left(\frac{\vec{r}_{E\to Sat.}}{\|\vec{r}_{E\to Sat.}\|^3} - \frac{\vec{r}_{M\to Sat.}}{\|\vec{r}_{M\to Sat.}\|^3} \right) - \mu_S \left(\frac{\vec{r}_{E\to Sat.}}{\|\vec{r}_{E\to Sat.}\|^3} - \frac{\vec{r}_{S\to Sat.}}{\|\vec{r}_{S\to Sat.}\|^3} \right)$$

(35)

Gravity Gradient Torque

Gravity gradient torque is a moment imposed on the satellite due to the gravity field of the central body (e.g. Earth). The gravity gradient torque ($\vec{M}_g$) calculations used in POST2 assume the central body has a spherical mass distribution. Though the Earth's gravity field is modeled as an oblate spheroid, the gravity gradient torque calculations used in POST2 still provide a useful approximation. Here $\vec{M}_g$ is dependent on the inertia tensor (I), μ_E, and the

cartesian components of $\vec{r}_{E\rightarrow Sat.}$ with respect to the FM frame. The derivation of the gravity gradient torque is depicted in Eq. (37) and is expressed in the FM frame.

$$I = \begin{bmatrix} I_{xx} & -I_{xy} & -I_{xz} \\ -I_{xy} & I_{yy} & -I_{yz} \\ -I_{xz} & -I_{yz} & I_{zz} \end{bmatrix} \tag{36}$$

$$\vec{M}_g = \frac{3\mu_E}{(X_{FM}^2 + Y_{FM}^2 + Z_{FM}^2)^{2.5}} (\vec{r}_{E\rightarrow Sat.} \times I\, \vec{r}_{E\rightarrow Sat.}) \tag{37}$$

EQUATIONS OF MOTION

Frame Transformations

The direction cosine matrix (DCM) that transforms the ECI frame to the flight mechanic frame is represented in Eq. (38). Here $\cos(\phi)$ and $\sin(\phi)$ are abbreviated by $c\phi$ and $s\phi$ respectively.

$$\mathrm{H}_{eci/fm} = \begin{bmatrix} \mathrm{c}\theta\ \mathrm{c}\psi & \mathrm{c}\theta\ \mathrm{s}\psi & -\mathrm{s}\theta \\ s\phi\ s\theta\ \mathrm{c}\psi - c\phi\ \mathrm{s}\psi & s\phi\ s\theta\ \mathrm{s}\psi + c\phi\ \mathrm{c}\psi & s\phi\ c\theta \\ c\phi\ s\theta\ \mathrm{c}\psi + \mathrm{s}\phi\ \mathrm{s}\psi & c\phi\ s\theta\ \mathrm{s}\psi - \mathrm{s}\phi\ \mathrm{c}\psi & c\phi\ c\theta \end{bmatrix} \tag{38}$$

The DCM that transforms states from EME 2000 to ECI is done via SPICE in POST2. SPICE translates Earth orientation data available from The Navigation and Ancillary Information Facility in the form of binary files. These files provide orientation data for Earth-centered inertial frame relative to the EME 2000 frame and produces its DCM ($H_{eme/eci}$) for POST2 at the given initial epoch.

$$H_{ecr/eci} = \begin{bmatrix} \cos(\omega_E \Delta\mathrm{t}) & \sin(\omega_E \Delta\mathrm{t}) & 0 \\ -\sin(\omega_E \Delta\mathrm{t}) & \cos(\omega_E \Delta\mathrm{t}) & 0 \\ 0 & 0 & 1 \end{bmatrix} \tag{39}$$

The DCM that transforms the ECI frame to the ECR frame is a function of time ($\Delta\mathrm{t}$) and the Earth's rotational constant (ω_E) as shown in Eq. (39).

Translational Acceleration (FM Frame)

The forces being modeled within the POST2 simulation are the forces from solar radiation pressure, Earth's oblate gravity field, and 3rd body perturbations from the Sun and Moon. The sum of those forces divided by the satellite's mass and transformed into the Flight Mechanic frame yields Eq. (40).

$$\vec{a}_{fm} = \frac{1}{M} F_s + H_{eci/fm} H_{ecr/eci} \vec{a}_g + H_{eci/fm} H_{eme/eci} \vec{a}_{3B} \quad (40)$$

Angular Accelerations (FM Frame)

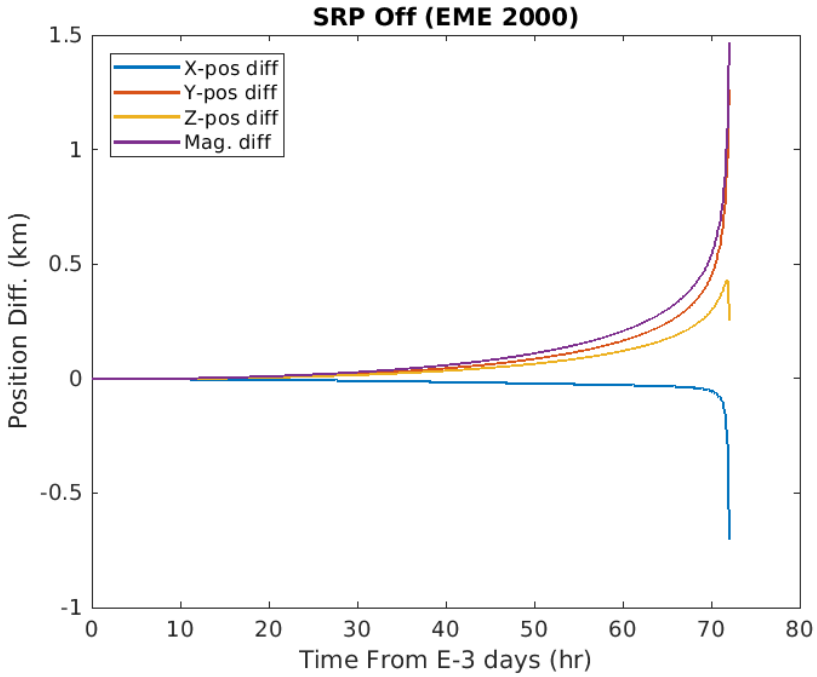
The moments being modeled within the POST2 simulation are the moments from solar radiation pressure and the gravity gradient torque. The sum of moments is shown in Eq. (41). With the sum of moments, inertias and angular velocities known, the angular accelerations can be calculated as see in Eq. (42).

$$\vec{M}_{fm} = \vec{M}_s + \vec{M}_g \quad (41)$$

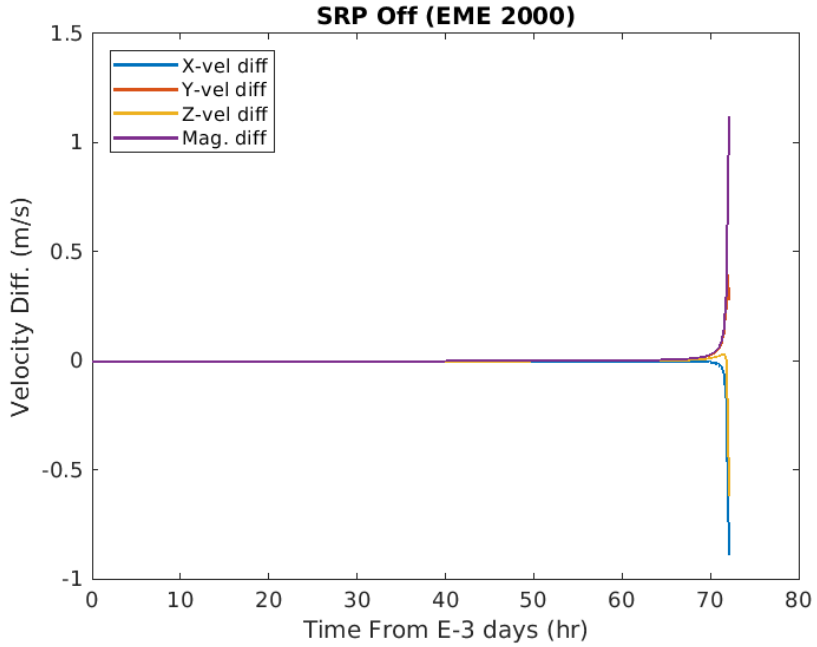
$$\vec{\alpha}_{fm} = I^{-1}\left(\vec{M}_{fm} - \vec{\omega}_{fm} \times I\vec{\omega}_{fm}\right) \quad (42)$$

RESULTS

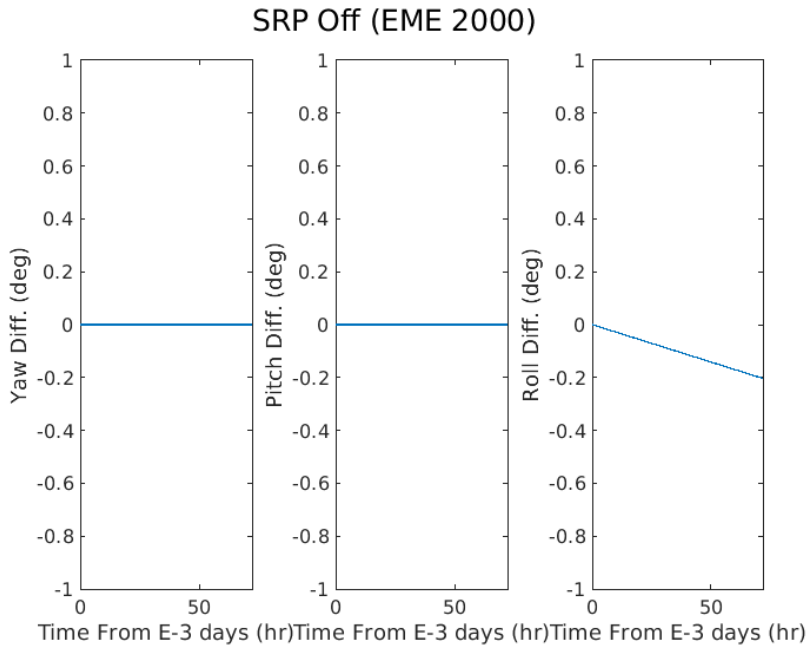
42 vs. POST2 (No SRP Forces and Moments)



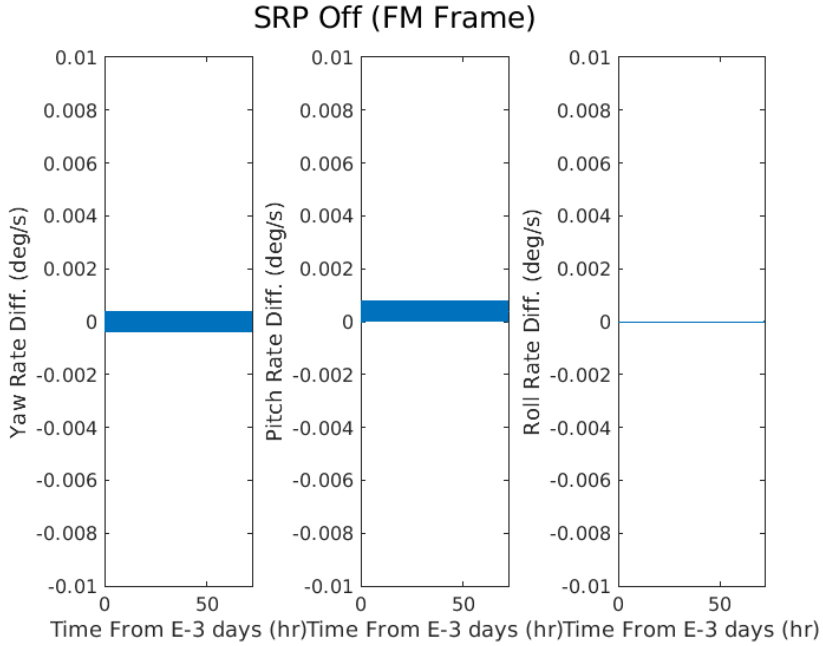
Graph 1: Position Difference (42 vs. POST2)



Graph 2: Velocity Difference (42 vs. POST2)



Graph 3: Euler Angle Differences (42 vs. POST2)



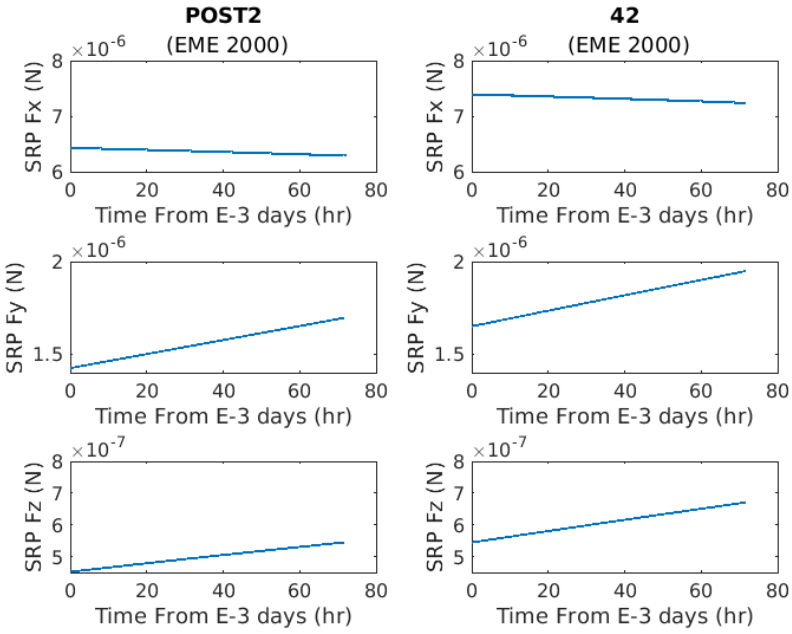
Graph 4: Euler Rate Differences (42 vs. POST2)

Vehicle State	Units	Relative Difference at End of Simulation
X-Pos.	km	-0.7066
Y-Pos.	km	1.2628
Z-Pos.	km	0.4316
Position Magnitude	km	1.4689
Velocity Magnitude	m/s	1.1260
Yaw	deg	1.791E-03
Pitch	deg	1.396E-03
Roll	deg	2.038E-01
Yaw Rate	deg/s	3.80E-04
Pitch Rate	deg/s	7.61E-04
Roll Rate	deg/s	3.31E-09

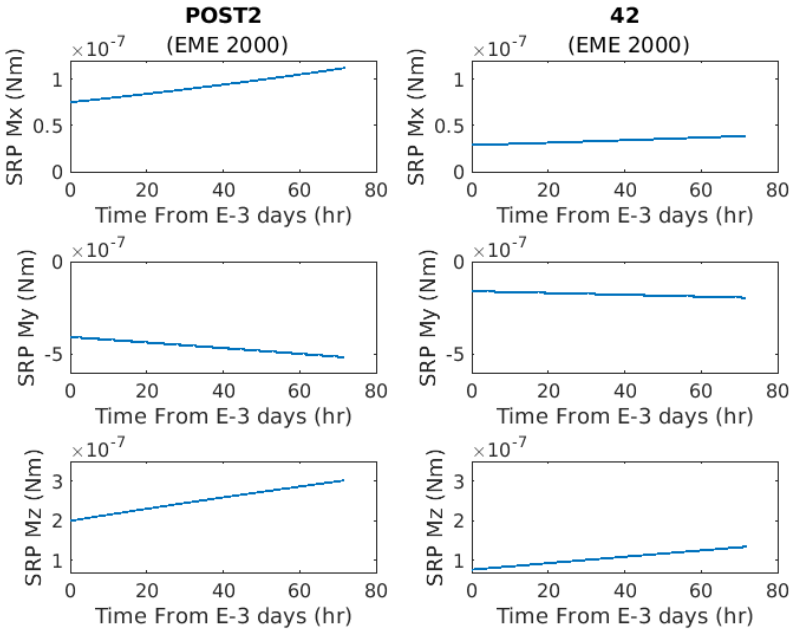
Table 2: 42 vs. POST2 Summary (SRP Off)

The differences between the Euler angles and rates appear to be in good agreement between the 42 and POST2 simulation. The components of velocity are in good agreement between the two simulations despite the unexplained spike that appears in the last hour of the trajectory. The differences in position appear to be more significant and is likely due to a small difference in gravitational forces and ephemerides data compounded over time. An independent comparison was done between 42 and the MONTE simulation tool. The position and velocity differences between 42 and MONTE are found in Appendix 3 and are in family with the position and velocity results in table (2).

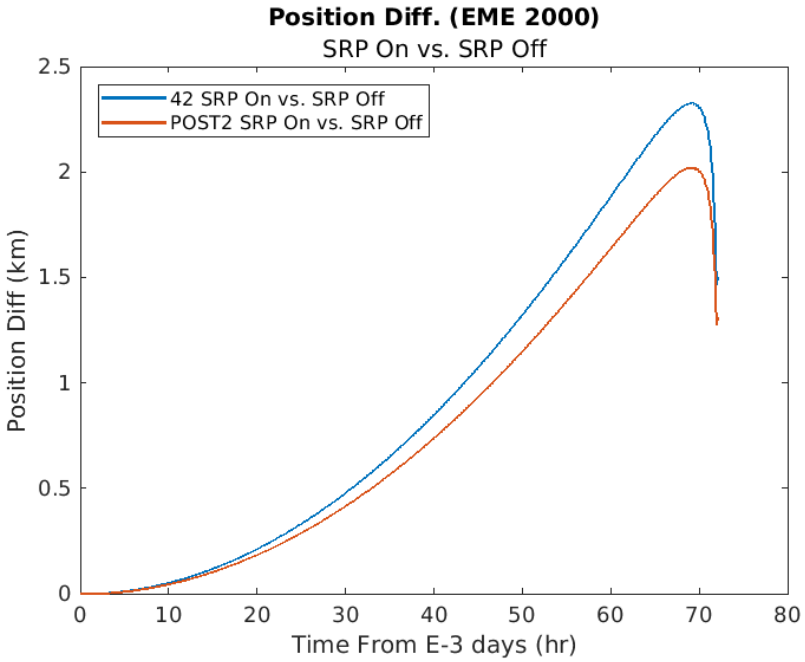
42 (SRP Method I) vs. POST2 (SRP Method II)



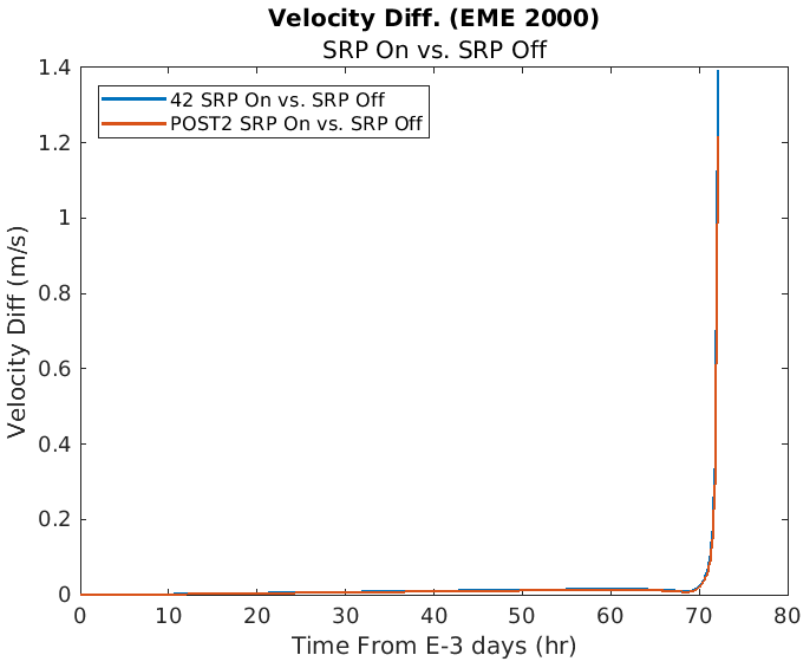
Graph 5:SRP Forces (Method I vs. Method II)



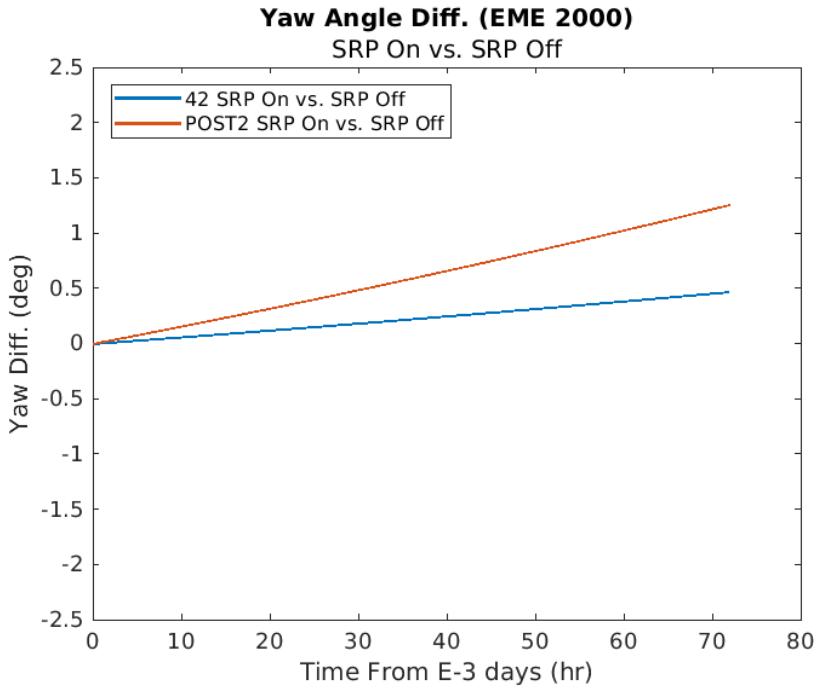
Graph 6: SRP Moments (Method I vs. Method II)



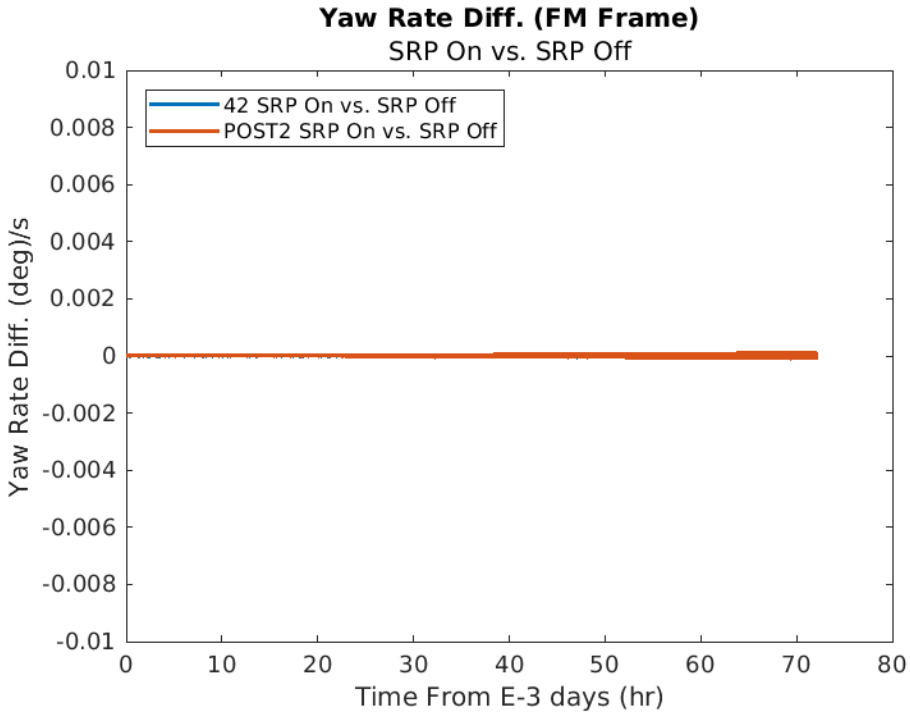
Graph 7: Position Difference (Method I vs. Method II)



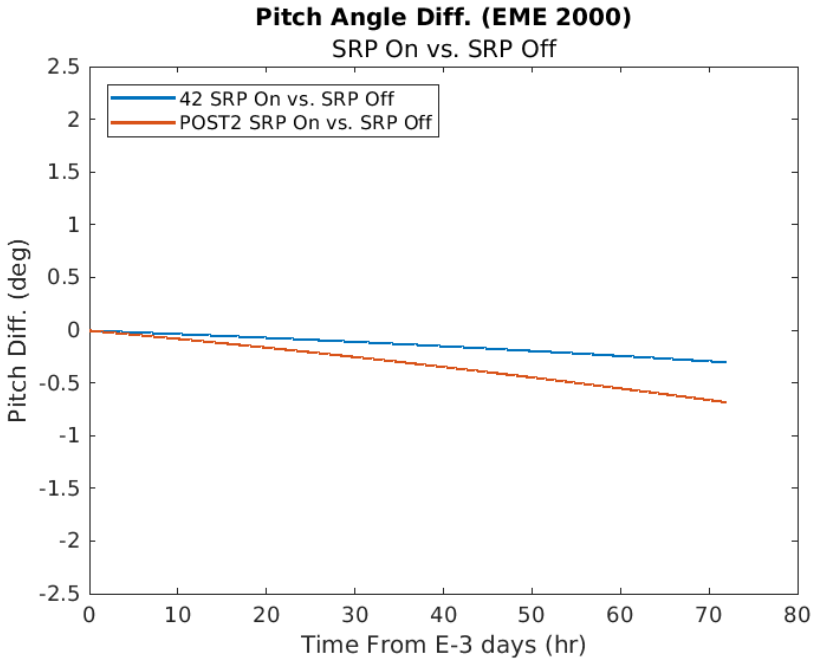
Graph 8: Velocity Difference (Method I vs. Method II)



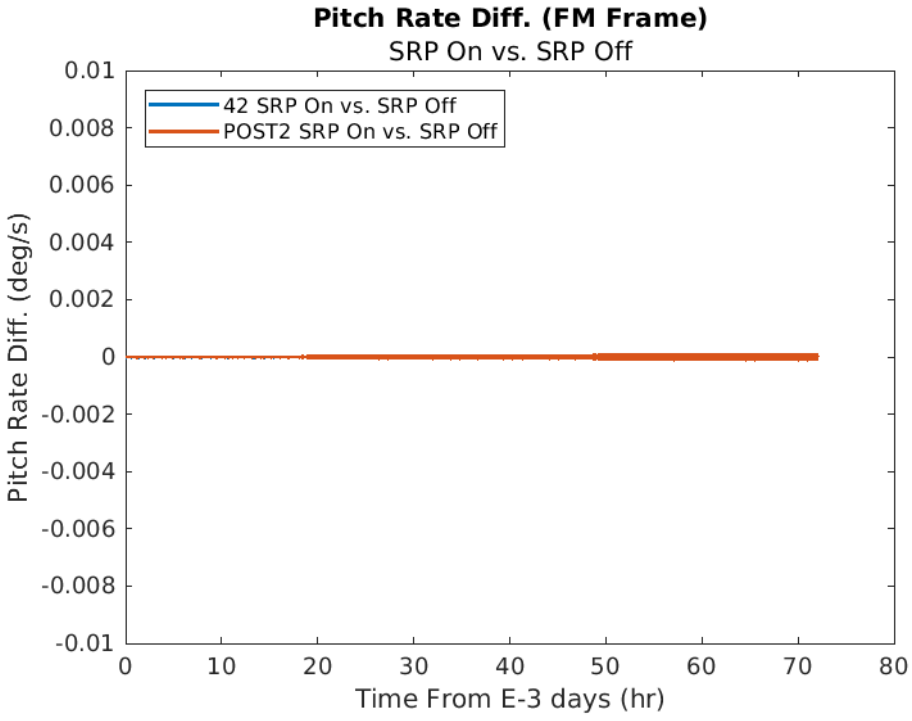
Graph 9: Yaw Difference (Method I vs. Method II)



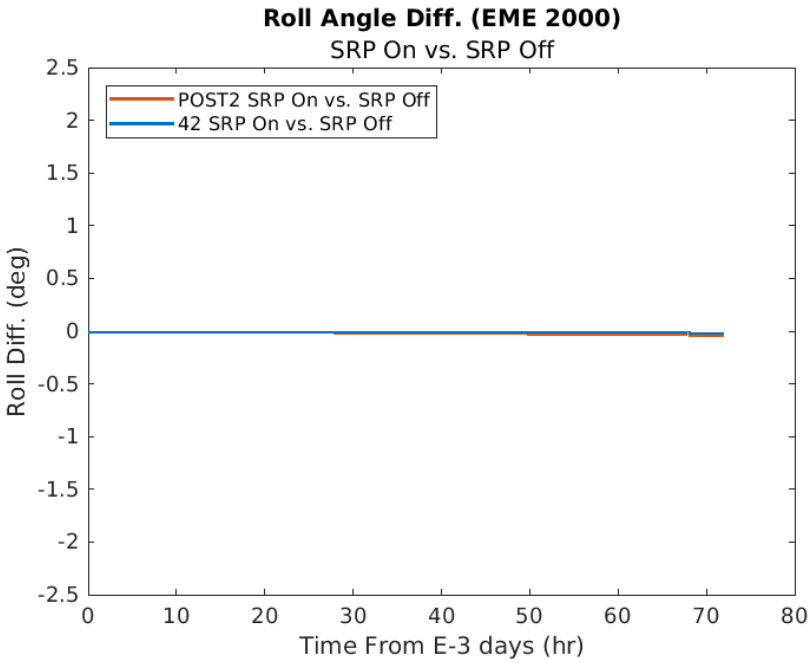
Graph 10: Yaw Rate Difference (Method I vs. Method II)



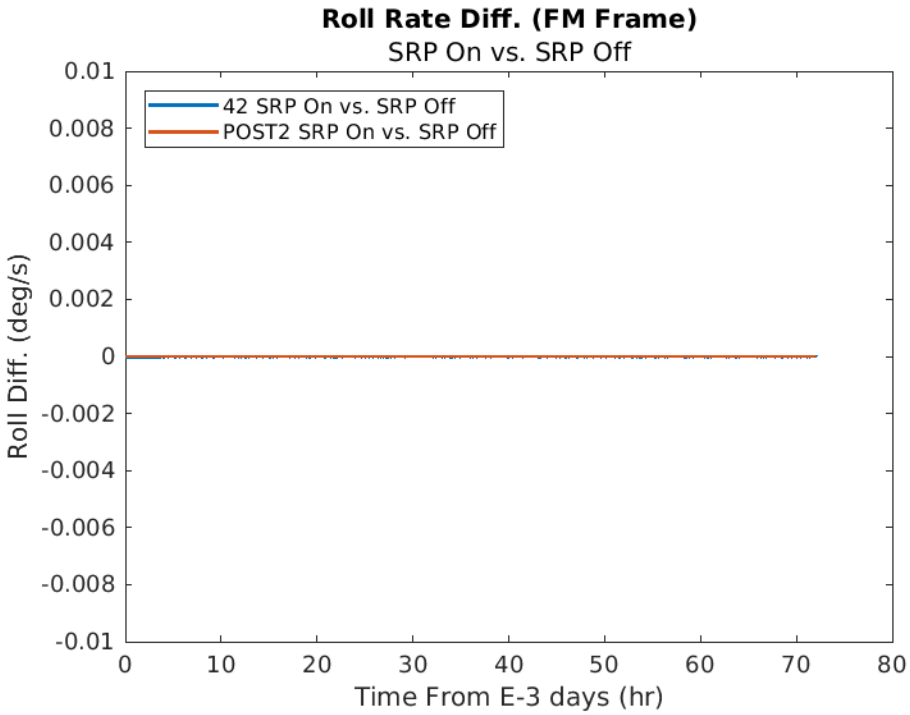
Graph 11: Pitch Difference (Method I vs. Method II)



Graph 12: Pitch Rate Difference (Method I vs. Method II)



Graph 13: Roll Difference (Method I vs. Method II)



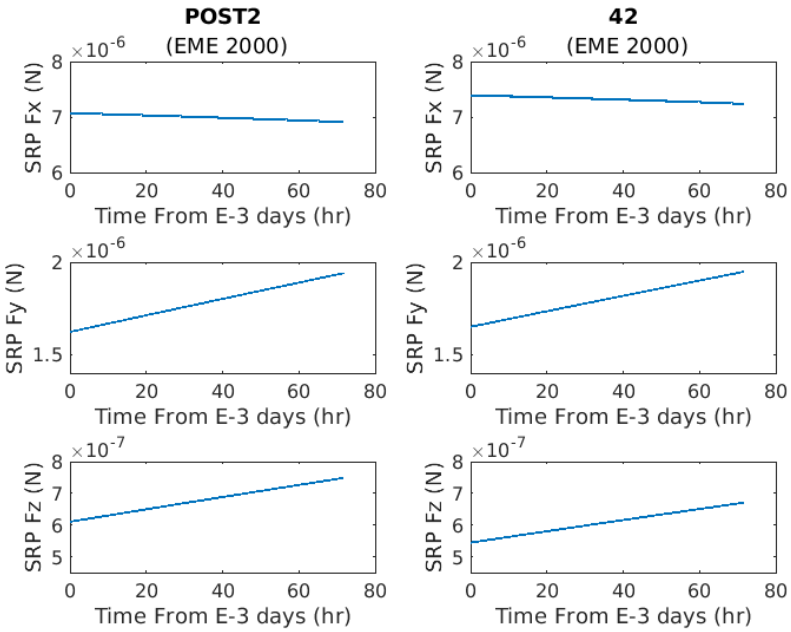
Graph 14: Roll Rate Difference (Method I vs. Method II)

Vehicle State	Units	42 (Method I) Relative Difference at End of Simulation	POST2 (Method II: Sphere-cone) Relative Difference at End of Simulation
SRP Fx	N	7.2462E-06	6.2970E-06
SRP Fy	N	1.9523E-06	1.6997E-06
SRP Fz	N	6.7222E-07	5.4631E-07
SRP Mx	Nm	3.9370E-08	1.1284E-07
SRP My	Nm	-1.9311E-07	-5.1575E-07
SRP Mz	Nm	1.3649E-07	3.0403E-07
Position Magnitude	km	1.5053	1.3251
Velocity Magnitude	m/s	1.3939	1.2192
Yaw	deg	0.4689	1.2550
Pitch	deg	-0.3002	-0.6791
Roll	deg	-0.0119	-0.0360
Yaw Rate	deg/s	6.5836E-05	1.7400E-05
Pitch Rate	deg/s	-2.1152E-05	-6.2648E-06
Roll Rate	deg/s	5.6916E-10	1.5747E-09

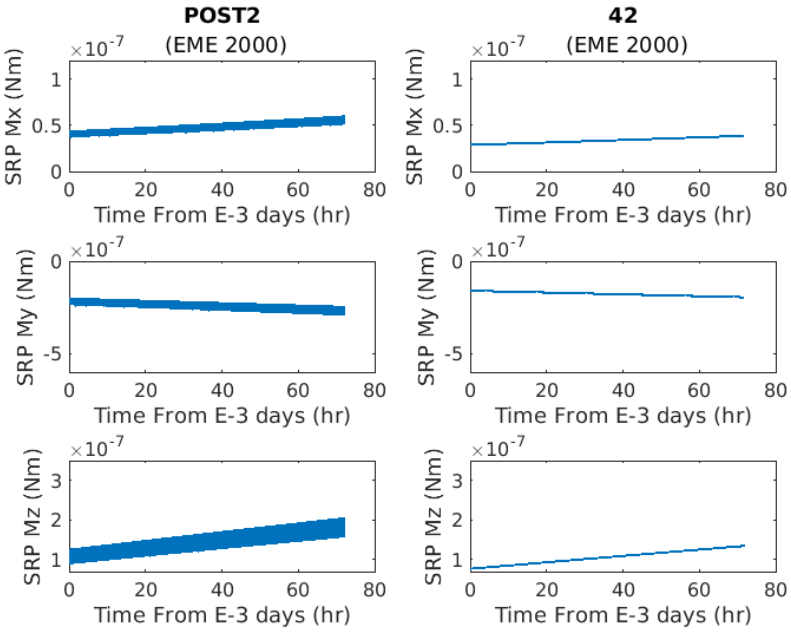
Table 3: 42 vs. POST2 Summary (Method I vs. Method II)

All metrics of interest are in relatively good agreement. Most of the error found between 42 and POST2 can be attributed to the small differences in gravitational error and ephemerides data used to define Sun, Moon, and Earth states.

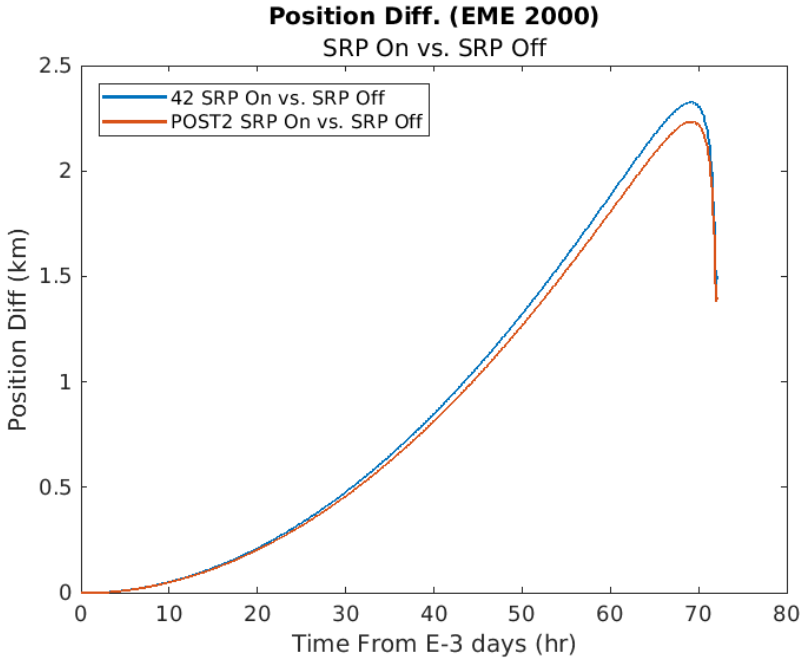
42 (SRP Method I) vs. POST2 (SRP Method III)



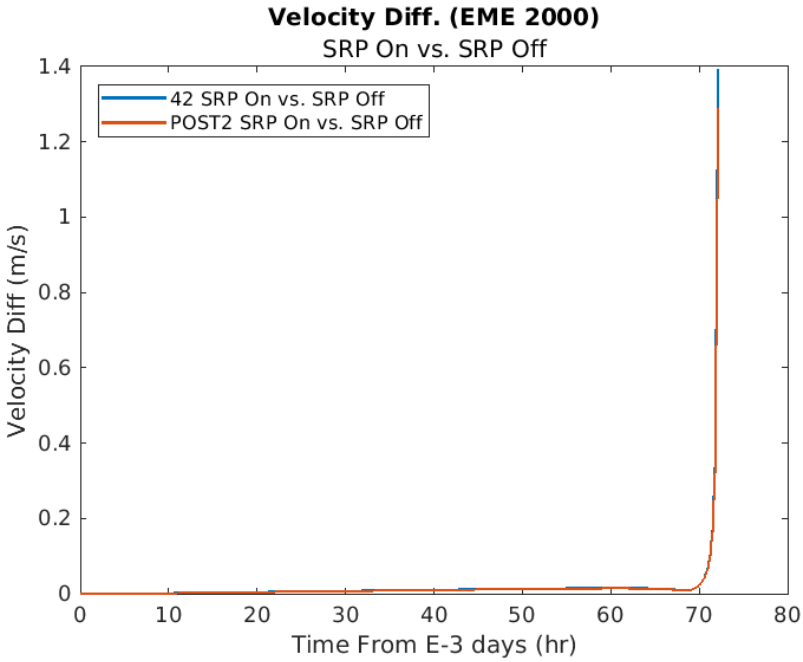
Graph 15: SRP Forces (Method I vs. Method III)



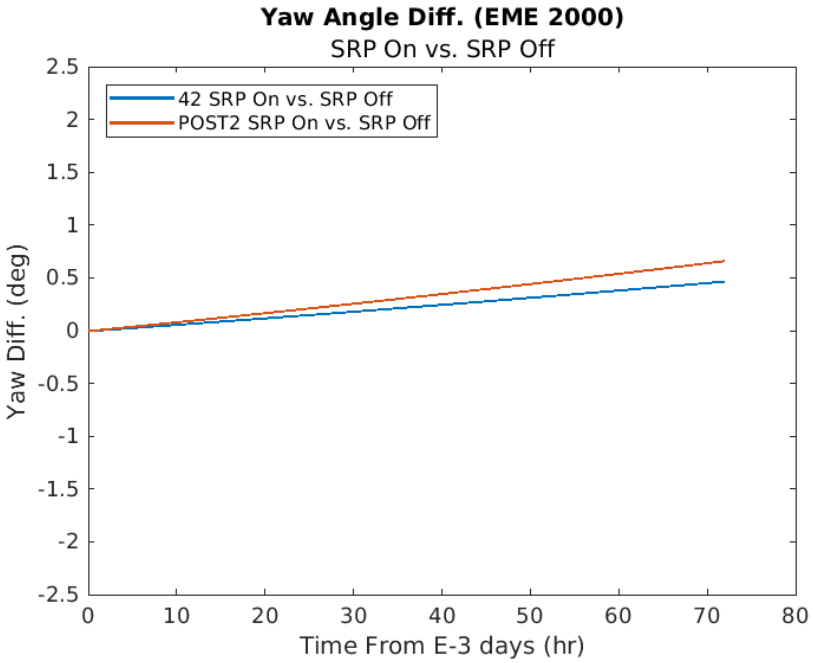
Graph 16: SRP Moments (Method I vs. Method III)



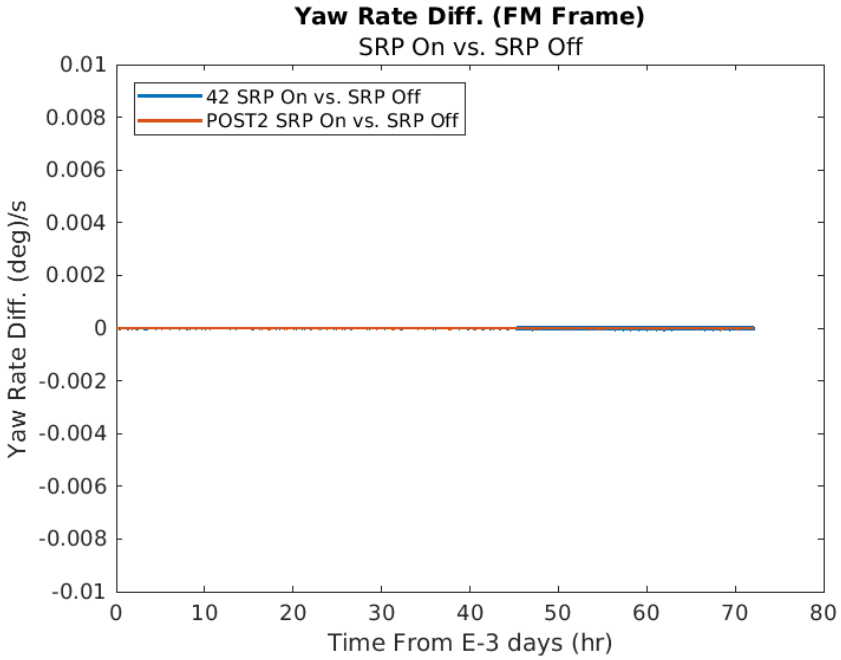
Graph 17:Position Difference (Method I vs. Method III)



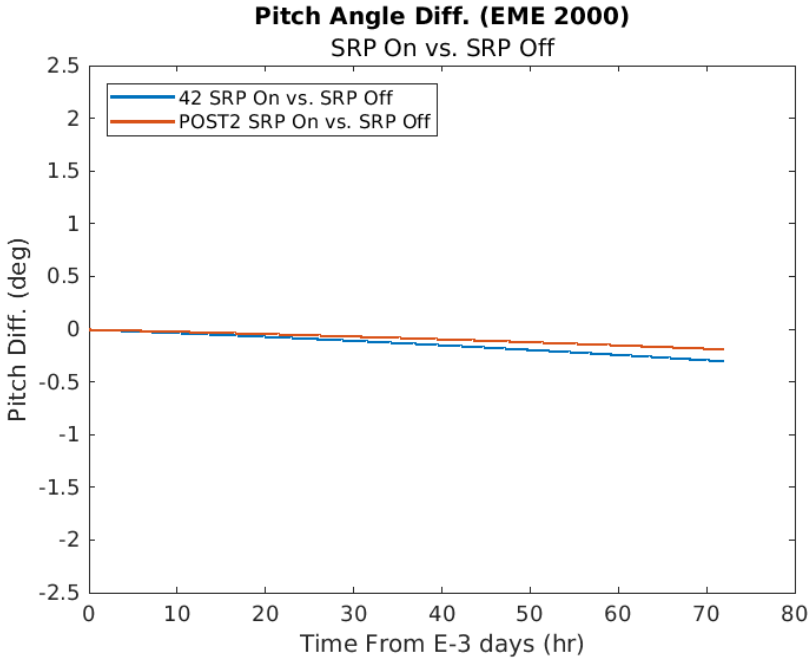
Graph 18: Velocity Difference (Method I vs. Method III)



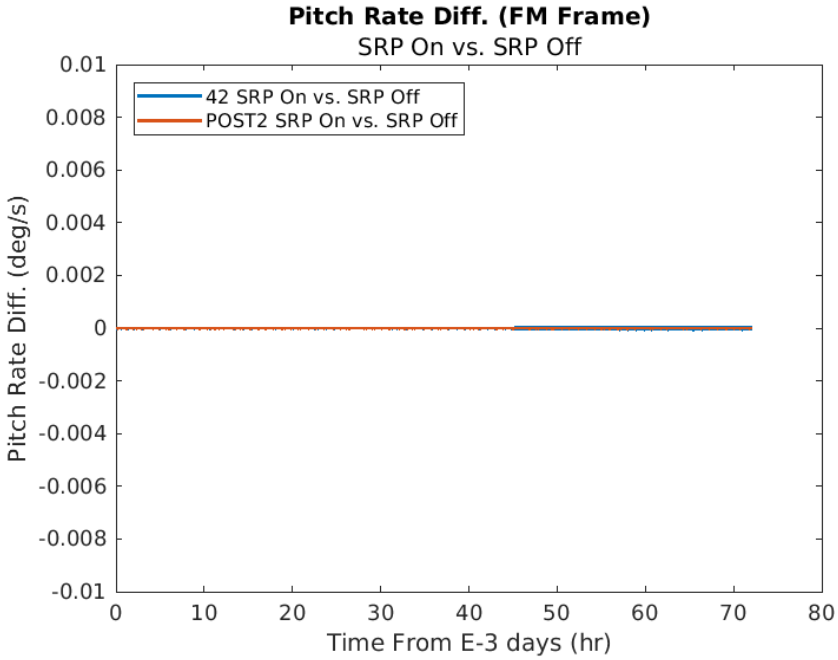
Graph 19: Yaw Difference (Method I vs. Method III)



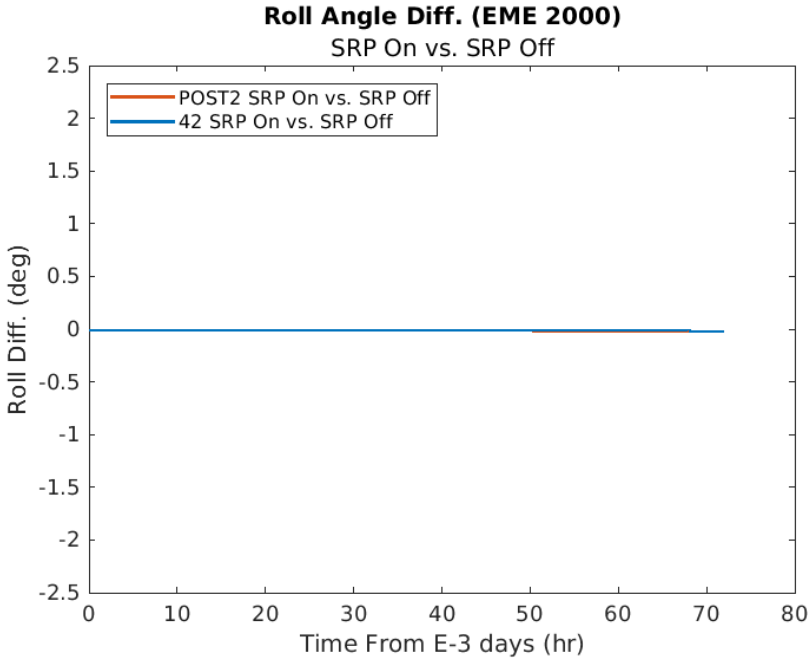
Graph 20: Yaw Rate Difference (Method I vs. Method III)



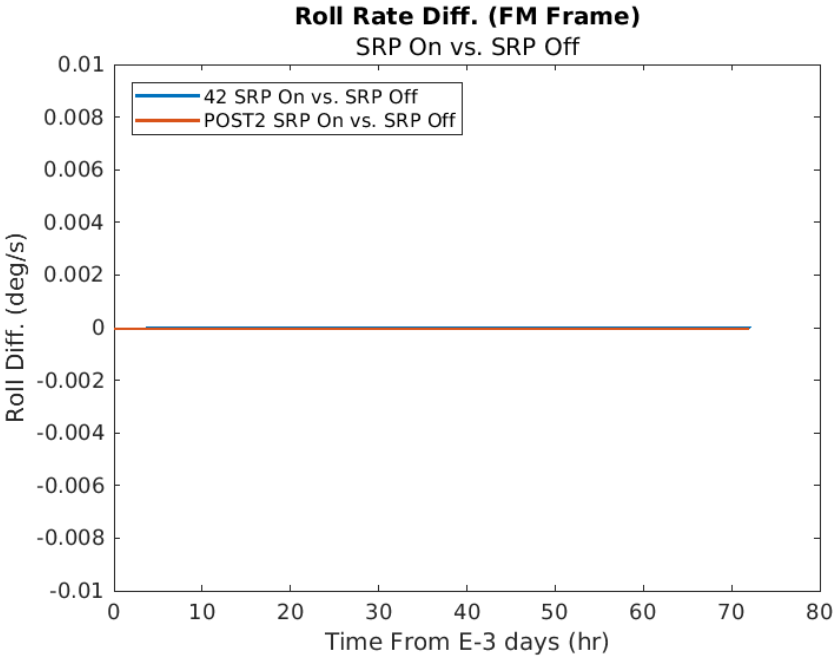
Graph 21: Pitch Difference (Method I vs. Method III)



Graph 22: Pitch Rate Difference (Method I vs. Method III)



Graph 23: Roll Difference (Method I vs. Method III)



Graph 24: Roll Rate Difference (Method I vs. Method III)

Vehicle State	Units	42 (Method I) Relative Difference at End of Simulation	POST2 (Method III: Sphere) Relative Difference at End of Simulation
SRP Fx	N	7.2462E-06	6.9180E-06
SRP Fy	N	1.9523E-06	1.9444E-06
SRP Fz	N	6.7222E-07	7.5038E-07
SRP Mx	Nm	3.9370E-08	5.9086E-08
SRP My	Nm	-1.9311E-07	-2.8299E-07
SRP Mz	Nm	1.3649E-07	2.0062E-07
Position Magnitude	km	1.5053	1.4034
Velocity Magnitude	m/s	1.3939	1.2911
Yaw	deg	0.4689	0.6626
Pitch	deg	-0.3002	-0.3887
Roll	deg	-0.0119	-0.0171
Yaw Rate	deg/s	6.5836E-05	9.4776E-05
Pitch Rate	deg/s	-2.1152E-05	1.0969-06
Roll Rate	deg/s	5.6916E-10	2.7850E-09

Table 4: 42 vs. POST2 Summary (Method I vs. Method III)

Results between 42's SRP modeling and POST2's SRP modeling show similar results compared to table (3). The similarities between table (3) and table (4) show that the approximating the POST2 vehicle as a sphere vs. a sphere-cone yields small but no significant difference during the simulated 72-hour trajectory.

CONCLUSION

The first objective of this project was to successfully compare the 42 trajectory solutions of the 72-hour exoatmospheric trajectory with POST2 without including SRP forces and moments. Overall, this objective has been met. The most significant difference between the 42 and POST2 simulations was a difference in position by ~1.47 km by the end of the simulation. This difference is likely attributed small differences in gravitational forces and ephemerides data compounded over time. The independent comparison between 42 and MONTE show POST2 and MONTE would've likely had similar results if a direct comparison was done.

The second objective of this project was to utilize a methodology of incorporating forces and moments due to solar radiation pressure into POST2. Overall, this objective has also been met. The two approaches of approximating the vehicle geometry as a generalized sphere-cone and a sphere produced similar results when comparing the two methods. The generalized sphere produced slightly better results when comparing to 42 and is likely due to the consistently small angle between the solar vector and x-axis of the flight mechanic frame. The smaller the angle between the solar vector and x-axis of the flight mechanic frame, the more EES faces directly into the Sun. In this orientation, the surface of EES projected by the Sun would appear to be circular. This method of using generalized shapes to model SRP forces is appropriate for a project in its preliminary design phases. For projects at a more mature level of design, a method such as 42 should be utilized to offer more fidelity.

Future Work

More testing is needed to determine the sensitivity attitude has on the POST2 SRP modeling. In this simulation, the angle between the EES flight mechanic frame x-axis and the solar vector vary only $\pm 10°$ around $0°$. Additionally, the SRP methods that were integrated into

POST2 assume that the vehicle is in constant view of the Sun. Additional work includes adding umbra and penumbra conditions in cases where the view of the Sun is blocked by another body. 42's SRP modeling incorporates umbra conditions and will be used utilized for comparisons in the future.

REFERENCES

[1] NASA Office of Inspector General, "Audit of the Mars Sample Return Program," NASA, Washington, D.C., 2024.

[2] G. Cataldo, B. Childs, C. Jim, B. Feehan, P. Gage, J. Lin, S. Mukherjee, M. Neuman, F. Pellerano, B. Sarli, C. Szalai, L. Teeney, J. Vander Kam, T. White, C. Yew and C. Zumwalt, "Mars Sample Return - An Overview of the Capture, Containment and Return System," in *IAF*, Paris, France, 2022.

[3] K. A. Hart, "Analytic Aerodynamic and Solar Radiation Pressure Modeling of Resident Space Objects," Georgia Institute of Technology, Atlanta, 2015.

[4] "Spherical Harmonic Representation of the Gravity Field Potential," [Online]. Available: https://spsweb.fltops.jpl.nasa.gov/portaldataops/mpg/MPG_Docs/Source%20Docs/gravity-SphericalHarmonics.pdf. [Accessed 1 March 2024].

[5] "Gravity Recovery and Climate Experiment," 2013. [Online]. Available: https://www2.csr.utexas.edu/grace/gravity/. [Accessed 05 February 2023].

[6] M. Lara, A. J. Rosengren and E. Fantino, "Nonsingular recursion formulas for third-body perturbations in mean vectorial elements," *Astronomy and Astrophysics,* vol. 634, p. 9, 2020.

APPENDIX 1: POST2 Simulation Inputs

Vehicle Properties

	Units	Value	Description
M	kg	92.3	Vehicle mass
Xcg	m	0.256	Center of gravity position in Body frame x-direction
Ycg	m	-1.66E-05	Center of gravity position in Body frame y-direction
Zcg	m	-3.28E-05	Center of gravity position in Body frame z-direction
Ixx	kg*m^2	9.97	X-axis moment of inertia
Iyy	kg*m^2	6.14	Y-axis moment of inertia
Izz	kg*m^2	6.13	Z-axis moment of inertia
Ixy	kg*m^2	2.28E-05	X and Y-axes product of inertia
Ixz	kg*m^2	1.29E-04	X and Z-axes product of inertia
Iyz	kg*m^2	-1.70E-05	Y and Z-axes product of inertia
R_n	m	0.31	Radius of spherical section of vehicle
R_c	m	0.625	Radius of cone section of vehicle
δ	deg	52.5	Half-cone angle of vehicle
C_{sr}	-	0.11	Solar specular reflection coefficient used for SRP calculations
C_{dr}	-	0.64	Solar diffusive reflection coefficient used for SRP calculations

Table 5: Vehicle Properties

Initial Vehicle States

	Units	Value	Description
X_{J2000}	km	-30058	X-component of vehicle position in EME 2000 frame
Y_{J2000}	km	-821901	Y-component of vehicle position in EME 2000 frame
Z_{J2000}	km	-581204	Z-component of vehicle position in EME 2000 frame
VX_{J2000}	km/s	0.17	X-component of vehicle velocity in EME 2000 frame
VY_{J2000}	km/s	2.9	Y-component of vehicle velocity in EME 2000 frame
VZ_{J2000}	km/s	2.1	Z-component of vehicle velocity in EME 2000 frame
ϕ	deg	45.1	Roll angle of FM frame with respect to EME 2000 frame
Θ	deg	-1.3	Pitch angle of FM frame with respect to EME 2000 frame
ψ	deg	-170.1	Yaw angle of FM frame with respect to EME 2000 frame
ω_x	deg/s	31.8	X-component of vehicle angular velocity in FM frame
ω_y	deg/s	0	Y-component of vehicle angular velocity in FM frame
ω_z	deg/s	0	Z-component of vehicle angular velocity in FM frame

Table 6: EES Initial States

Planetary Constants

	Units	Value	Description
a_e	m	6378137	Semi-major axis of the Earth's reference ellipsoid
μ_E	m^3/s^2	3.986E+14	Earth gravitational constant
μ_S	m^3/s^2	1.327E+20	Sun gravitational constant
μ_M	m^3/s^2	4.903E+12	Moon gravitational constant
ω_E	rad/s	7.292E-05	Earth rotational constant

Table 7: Planetary Constants

Miscellaneous Constants

	Units	Value	Description
k_{1AU}	W/m^2	1366.1	Solar flux at 1 astronomical unit (AU)
AU	km	1.4959E+08	Mean distance of Earth from Sun
c	km/s	2.9979E+05	Speed of light

Table 8: Misc. Constants

Gravitational Harmonic Coefficients

ℓ	m	$C_{\ell,m}$	$S_{\ell,m}$
0	0	1.000000000000e+00	0.000000000000e+00
1	0	0.000000000000e+00	0.000000000000e+00
1	1	0.000000000000e+00	0.000000000000e+00
2	0	-4.841694573200e-04	0.000000000000e+00
2	1	-3.183715553800e-10	1.432170507577e-09
2	2	2.439374598584e-06	-1.400287554684e-06
3	0	9.571739577330e-07	0.000000000000e+00
3	1	2.030447717179e-06	2.482356432550e-07
3	2	9.047749228904e-07	-6.190079043255e-07
3	3	7.212923883714e-07	1.414398684143e-06
4	0	5.399853533873e-07	0.000000000000e+00
4	1	-5.361786622025e-07	-4.735770747989e-07
4	2	3.504917311439e-07	6.625021916813e-07
4	3	9.908574388920e-07	-2.009475655717e-07
4	4	-1.884904077578e-07	3.088195368429e-07
5	0	6.865295795743e-08	0.000000000000e+00
5	1	-6.291443819205e-08	-9.434270766598e-08
5	2	6.520588473561e-07	-3.233441597218e-07
5	3	-4.518301141322e-07	-2.149419060333e-07
5	4	-2.953263261931e-07	4.981208263958e-08
5	5	1.748131765178e-07	-6.693584989617e-07
6	0	-1.499751867421e-07	0.000000000000e+00
6	1	-7.594321204929e-08	2.652551908729e-08
6	2	4.863521615052e-08	-3.737703607081e-07
6	3	5.724955887621e-08	8.973058346979e-09
6	4	-8.599819097325e-08	-4.714267493844e-07
6	5	-2.671626945449e-07	-5.364950882609e-07
6	6	9.476848430257e-09	-2.373833884330e-07
7	0	9.050171042435e-08	0.000000000000e+00
7	1	2.808863583475e-07	9.515955090460e-08
7	2	3.303956821278e-07	9.302002881123e-08
7	3	2.504641688786e-07	-2.170971014715e-07
7	4	-2.749881969827e-07	-1.240495513726e-07
7	5	1.646915418368e-09	1.793002894971e-08
7	6	-3.587987635262e-07	1.517944882424e-07
7	7	1.520997456997e-09	2.410335977031e-08
8	0	4.947888296780e-08	0.000000000000e+00

8	1	2.314094409863e-08	5.890481663055e-08
8	2	8.002052911833e-08	6.529987615773e-08
8	3	-1.936026267135e-08	-8.594160265972e-08
8	4	-2.443452151910e-07	6.981209020667e-08
8	5	-2.570144866932e-08	8.920688936506e-08
8	6	-6.597081184471e-08	3.089447805354e-07
8	7	6.725636222065e-08	7.486454436427e-08
8	8	-1.240327183045e-07	1.205413610615e-07
9	0	2.802321300936e-08	0.000000000000e+00
9	1	1.421492928072e-07	2.141577882289e-08
9	2	2.141197338560e-08	-3.168024895137e-08
9	3	-1.606019573082e-07	-7.425004177984e-08
9	4	-9.350161489798e-09	1.989919559209e-08
9	5	-1.631497881592e-08	-5.404368530546e-08
9	6	6.278398028405e-08	2.229639832314e-07
9	7	-1.179817162200e-07	-9.692085557350e-08
9	8	1.881308400622e-07	-3.004312450334e-09
9	9	-4.755850838420e-08	9.687679926414e-08
10	0	5.334548503766e-08	0.000000000000e+00
10	1	8.375363375701e-08	-1.310944029602e-07
10	2	-9.397776594947e-08	-5.126508453457e-08
10	3	-6.991782448910e-09	-1.541282086692e-07
10	4	-8.445953067724e-08	-7.902406566030e-08
10	5	-4.928512438848e-08	-5.061658986031e-08
10	6	-3.758689850031e-08	-7.977130839748e-08
10	7	8.257212389859e-09	-3.049080805774e-09
10	8	4.058896471120e-08	-9.171058318062e-08
10	9	1.253844452739e-07	-3.794235151694e-08
10	10	1.004226496670e-07	-2.386171438519e-08
11	0	-5.076471651592e-08	0.000000000000e+00
11	1	1.561445511870e-08	-2.712116973592e-08
11	2	2.011370235930e-08	-9.898792206508e-08
11	3	-3.057064924138e-08	-1.488319687843e-07
11	4	-3.794141857164e-08	-6.376629453539e-08
11	5	3.741833595850e-08	4.958579381444e-08
11	6	-1.567706598770e-09	3.427333823533e-08
11	7	4.656483756694e-09	-8.982763203531e-08
11	8	-6.312532166228e-09	2.454717007194e-08
11	9	-3.107684181782e-08	4.206445252696e-08
11	10	-5.223715786334e-08	-1.841902381775e-08
11	11	4.623417376361e-08	-6.967214077592e-08
12	0	3.644772198802e-08	0.000000000000e+00
12	1	-5.358832704831e-08	-4.316858026027e-08
12	2	1.427947122528e-08	3.109996755745e-08
12	3	3.963402759354e-08	2.506888259894e-08

12	4	-6.772124976957e-08	3.838595095629e-09
12	5	3.087516986732e-08	7.588619712140e-09
12	6	3.132533350112e-09	3.897913732025e-08
12	7	-1.905584829350e-08	3.572403419363e-08
12	8	-2.588863528111e-08	1.693607739397e-08
12	9	4.191018338547e-08	2.496066882244e-08
12	10	-6.199792120952e-09	3.093616590226e-08
12	11	1.136453867516e-08	-6.387979602617e-09
12	12	-2.422093764787e-09	-1.111081244643e-08
13	0	4.173108178960e-08	0.000000000000e+00
13	1	-5.144214312313e-08	3.868433772835e-08
13	2	5.530911493830e-08	-6.268632741087e-08
13	3	-2.155183552058e-08	9.768544008057e-08
13	4	-3.643530335840e-09	-1.175327933577e-08
13	5	5.836923554071e-08	6.722112266360e-08
13	6	-3.504391341304e-08	-6.275311845657e-09
13	7	3.011217535175e-09	-7.322709449605e-09
13	8	-1.005495235818e-08	-9.856033661191e-09
13	9	2.476918342476e-08	4.588766543898e-08
13	10	4.111060619370e-08	-3.684174648755e-08
13	11	-4.452294971096e-08	-4.842840844923e-09
13	12	-3.131090717263e-08	8.793994419008e-08
13	13	-6.120785064008e-08	6.814809689050e-08
14	0	-2.266255103173e-08	0.000000000000e+00
14	1	-1.876921419784e-08	2.886037818844e-08
14	2	-3.591303253395e-08	-4.061905845524e-09
14	3	3.652390657012e-08	1.969523101268e-08
14	4	1.610649161708e-09	-2.266366589970e-08
14	5	2.931078216421e-08	-1.678909385480e-08
14	6	-1.906618605297e-08	2.453579955441e-09
14	7	3.762574388904e-08	-3.934832237839e-09
14	8	-3.494636316883e-08	-1.544593008209e-08
14	9	3.195352534828e-08	2.846644222586e-08
14	10	3.879941283242e-08	-1.294046965893e-09
14	11	1.564776952490e-08	-3.904241899701e-08
14	12	8.460416301768e-09	-3.112727023506e-08
14	13	3.224257665829e-08	4.515011973925e-08
14	14	-5.187164013579e-08	-4.818313457120e-09
15	0	2.190523754540e-09	0.000000000000e+00
15	1	9.431691711573e-09	1.048058456956e-08
15	2	-2.053057809599e-08	-3.029749405778e-08
15	3	5.341468392835e-08	1.765566730691e-08
15	4	-4.016916883289e-08	6.808276487218e-09
15	5	1.224293540571e-08	7.616847169090e-09
15	6	3.285309257758e-08	-3.647002441656e-08

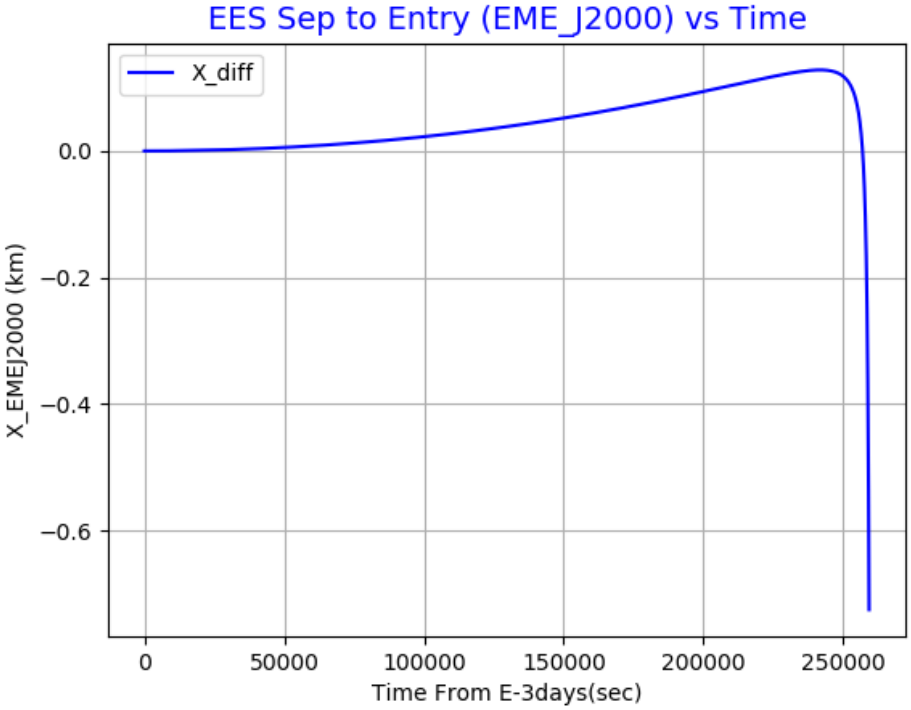
15	7	5.965424132107e-08	5.070720532234e-09
15	8	-3.209349570136e-08	2.217502570028e-08
15	9	1.329893002620e-08	3.799238450129e-08
15	10	1.026658425237e-08	1.469251823853e-08
15	11	-1.302365564589e-09	1.851979019599e-08
15	12	-3.241575455841e-08	1.560826198390e-08
15	13	-2.836827552207e-08	-4.576547774197e-09
15	14	5.197498227903e-09	-2.439524703504e-08
15	15	-1.902884996321e-08	-4.697544241010e-09
16	0	-4.707007538767e-09	0.000000000000e+00
16	1	2.618902007774e-08	3.334821083361e-08
16	2	-2.450511263015e-08	2.802488752940e-08
16	3	-3.390729558987e-08	-2.134077672470e-08
16	4	4.085456100372e-08	4.798913658255e-08
16	5	-1.212154058021e-08	-3.444879441362e-09
16	6	1.387144742207e-08	-3.559850771282e-08
16	7	-8.064228177193e-09	-8.654465267002e-09
16	8	-2.120827965186e-08	5.410326258238e-09
16	9	-2.241313365819e-08	-3.966774323340e-08
16	10	-1.180740182444e-08	1.153753078882e-08
16	11	1.911134519756e-08	-3.202184136285e-09
16	12	1.956574070056e-08	6.725805195288e-09
16	13	1.377368403739e-08	1.046349229027e-09
16	14	-1.934492676906e-08	-3.864833514437e-08
16	15	-1.441572316476e-08	-3.277196842439e-08
16	16	-3.830305243626e-08	2.968936758697e-09
17	0	1.918570569741e-08	0.000000000000e+00
17	1	-2.536685877499e-08	-3.170771148743e-08
17	2	-2.010186379896e-08	6.813694233382e-09
17	3	6.306652479273e-09	5.075494875520e-09
17	4	6.476272530891e-09	2.533200551418e-08
17	5	-1.621781571160e-08	8.027046264876e-09
17	6	-1.173247185573e-08	-2.944084158021e-08
17	7	2.497370105186e-08	-4.387399317237e-09
17	8	3.899494630615e-08	3.636082373825e-09
17	9	3.476630226507e-09	-2.764201385515e-08
17	10	-3.793708201514e-09	1.837877254420e-08
17	11	-1.601781359489e-08	1.108473143866e-08
17	12	2.872260876487e-08	2.045764071888e-08
17	13	1.650319119223e-08	2.013690236822e-08
17	14	-1.427370877457e-08	1.157256731622e-08
17	15	5.543850143403e-09	5.244699555808e-09
17	16	-3.040485227035e-08	3.606365353864e-09
17	17	-3.469931352117e-08	-1.986884587186e-08
18	0	6.099572825892e-09	0.000000000000e+00

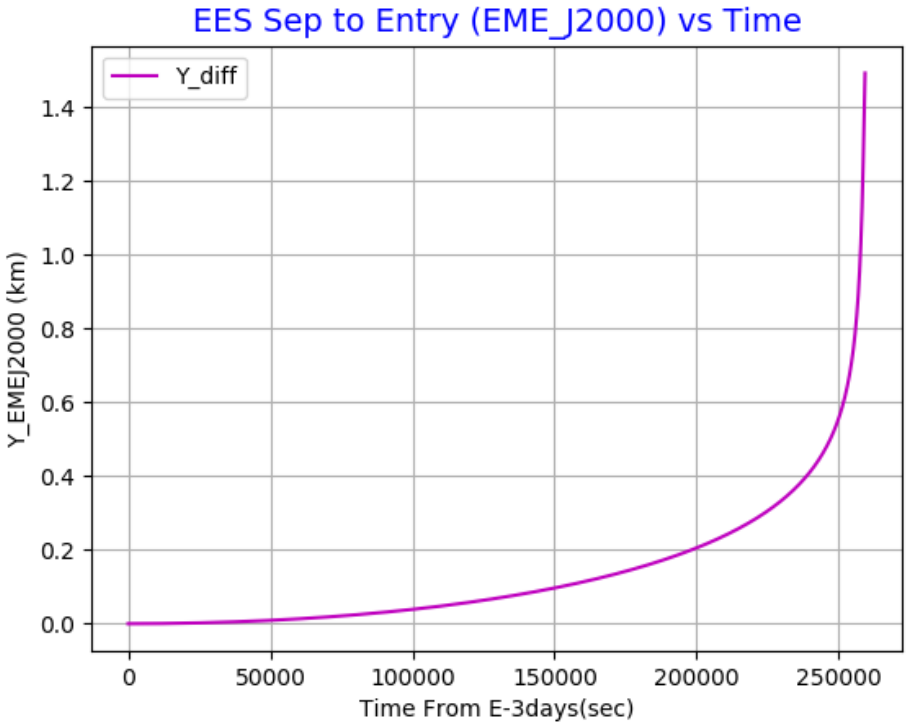
18	1	7.203784312131e-09	-3.928907023296e-08
18	2	1.472705760624e-08	1.082829870252e-08
18	3	-5.040994354023e-09	-5.853271924204e-09
18	4	5.462369118168e-08	-7.839385013683e-10
18	5	5.976729955829e-09	2.613745006950e-08
18	6	1.357585260390e-08	-1.324588484958e-08
18	7	6.792764103635e-09	7.465330691461e-09
18	8	3.049666090445e-08	4.346341593238e-09
18	9	-1.957016015145e-08	3.613284012470e-08
18	10	5.215322986070e-09	-4.240734806665e-09
18	11	-6.888150130208e-09	2.118398826541e-09
18	12	-2.974873074005e-08	-1.656358604851e-08
18	13	-6.254028731580e-09	-3.493744811846e-08
18	14	-8.294085837770e-09	-1.283057274104e-08
18	15	-4.046624145694e-08	-2.027734358671e-08
18	16	1.016275250768e-08	6.504438990004e-09
18	17	3.481621489201e-09	4.382747305204e-09
18	18	2.995484957740e-09	-1.084602918887e-08

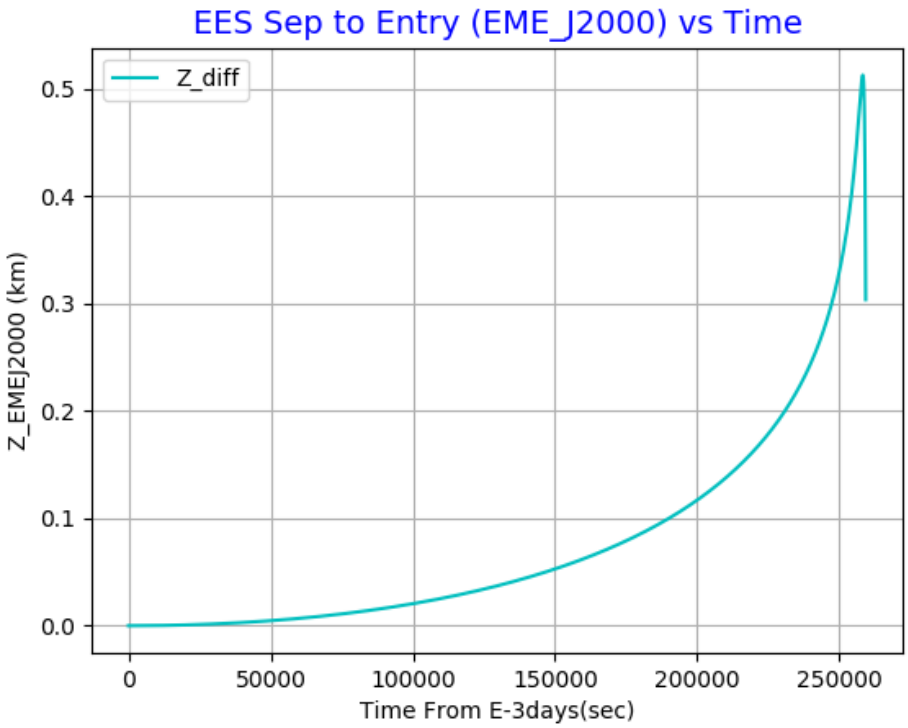
Table 9: Gravitational Harmonic Coefficients

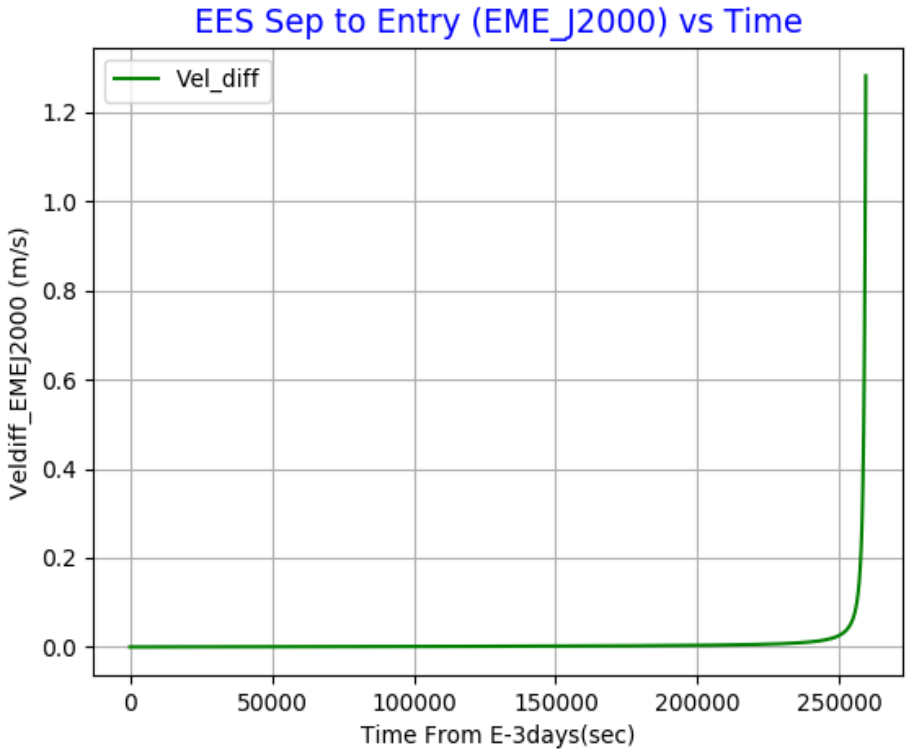
APPENDIX 2: 42 vs. MONTE Comparisons

Plots of Relative Difference






EES Sep to Entry (EME_J2000) vs Time
Z_diff
Z_EMEJ2000 (km)
0.0
0.1
0.2
0.3
0.4
0.5
0
50000
100000
150000
200000
250000
Time From E-3days(sec)


EES Sep to Entry (EME_J2000) vs Time
Vel_diff
Veldiff_EMEJ2000 (m/s)
0.0
0.2
0.4
0.6
0.8
1.0
1.2
0
50000
100000
150000
200000
250000
Time From E-3days(sec)

42 vs. MONTE Summary Table

Vehicle State	Units	Relative Difference at End of Simulation
X	km	-0.725
Y	km	1.494
Z	km	0.304
Position Magnitude	km	1.688
Velocity Magnitude	m/s	1.28